New developments of a multifrequency virtual spectrometer: stereo-electronic, dynamical and environmental effects on chiroptical spectra

Vincenzo Barone[a,*], Alberto Baiardi[a], Julien Bloino[a,b]
[a]: Scuola Normale Superiore, Piazza dei Cavalieri 7, 56126 Pisa, Italy
[b]: Consiglio Nazionale delle Ricerche, Istituto di Chimica dei Composti Organometallici, UOS di Pisa, Via G. Moruzzi 1, 56124 Pisa, Italy
[*]: Corresponding author: email: vincenzo.barone@sns.it

Keywords

Camphor; dimethyloxirane; solvent effects; anharmonic intensities; VPT2; Franck-Condon; Herzberg-Teller; Duschinsky effects

Abstract

Computational spectroscopy has recently evolved from a field reserved to specialists toward a general tool allowing interpretations and analyses of experimental results. However, the current practice of providing tables of transitions for rigid geometries, possibly tuned by phenomenological broadening is by far too naive. In order to improve this situation, in the last few years we have been developing a general, robust and user-friendly virtual spectrometer (VS) able to complement experimental studies for complex systems in condensed phases. The VS is based on flexible graphical pre- and post-processing tools interfaced with general number crunching software. This last tool is rooted on several electronic structure methodologies (DFT, TD-DFT, post-Hartree-Fock), powerful discrete/continuum models for describing environmental effects, and general vibrational and vibronic models. These last topics are the main focus of this work, which sketches our latest developments related to effective inclusion of anharmonic contributions, together with time-independent and/or time-dependent descriptions of vibronic transitions including Franck-Condon, Herzberg-Teller, and Duschinsky effects. Some test cases are described in some detail with the aim of showing the role of different effects in ruling vibrational (VCD) and electronic (ECD, CPL) chiral spectroscopies.

1 Introduction

Chiroptical spectroscopies are receiving increasing attention for the study of biological molecules where assignment of absolute configuration and characterization of physical-chemical properties are particularly significant in view of the completely different biological activity of molecules with the same basic composition, but centers of different chirality[1]. Among those spectroscopies circular dichroism (CD), i.e. the differential absorption of left- and right-handed circularly polarized light, has played a prominent role for the study of the absolute stereochemistry and conformation of chiral molecules[1-4]. However, in analogy with conventional one-photon spectroscopies, while vibrational (here vibrational circular dichroism, VCD) and electronic (here electronic circular dichroism, ECD) absorption spectra are able to characterize ground electronic states, emission spectra (here circularly polarized luminescence, CPL) are needed to unravel additional features of the excited electronic state from which the emission takes place. From an experimental point of view, while VCD and ECD have a quite consolidated history, CPL studies are much less widespread. In all cases, the information provided by experimental spectra can be significantly enhanced by companion quantum mechanical (QM) computations able to dissect the overall result in the different contributions of

stereo-electronic, dynamic, and environmental effects. In this connection the development of methods rooted in the density functional theory (DFT) and its time-dependent (TD-DFT) extension has revolutionized the field giving access to reliable computations of medium- to large-size flexible systems[5]. Although some limitations are still present and development of improved functionals is a very active research field[6-8], we already have at our disposal robust and reliable approaches at least for ground and valence excited states not involving too large multi-reference and/or charge transfer contributions (see Ref. [9] and references therein for examples of applications). At the same time, the polarizable continuum model (PCM)[10] allows reliable descriptions of bulk solvent effects without any appreciable increase of computational costs and can be effectively coupled to explicit descriptions of a reduced number of solvent molecules whenever specific effects (e.g. hydrogen bridges) require a more detailed description in the cybotactic region[11, 12]. The problem of dynamics is more involved and does not have a single well-defined solution for all kinds of problems. In our opinion, integrated approaches combining fully quantum mechanical descriptions of stiff degrees of freedom and classical (molecular dynamics, MD) descriptions of large amplitude intra- and intermolecular motions are particularly promising and are under active development[5]. Here we will concentrate on semi-rigid systems, which are reasonably described at the harmonic level, at most requiring a low-order perturbation treatment of anharmonic contributions. In the last few years we have developed a general, robust, and user-friendly virtual spectrometer for the accurate description of these systems concerning both vibrational[13-16](infra-red [IR], Raman, VCD) and vibronic[16-19](one photon absorption and emission [OPA and OPE], resonance raman [RR], ECD) spectroscopies. In particular, vibronic spectra can be computed by both time-independent (TI) and time-dependent (TD) approaches taking into account Franck-Condon, Herzberg-Teller, and Duschinsky effects. Furthermore the leading anharmonic contributions can be taken into account toward an extension of the vibrational second-order perturbation theory (VPT2)approach and solvent effects can be effectively included with the proper non equilibrium versions of the PCM[20], possibly adding also some explicit solvent molecule in the first solvation shell. We have now extended our spectrometer to CPL and in this paper we will show the first results of combined VCD, ECD, and CPL studies for some well-known systems (dimethyloxirane, (1R)-camphorquinone, (1S,4S)-bicyclo[2.2.2]octan-2,5-dione).

The paper is organized as follows. The first section is devoted to the general presentation of the virtual spectrometer and the theoretical background on which it is based. A short description of the computational protocol concludes this section. In the second section, we present some applications of the computational spectrometer with the aim of illustrating its most distinctive features and analyze its capacity to reproduce experimental results. A few concluding remarks on the spectrometer and the possibilities it offers to support the characterization of experimental spectra close this presentation.

2 Materials and Methods

2.1 Theoretical framework

The general theory and latest developments of our perturbative approach to anharmonic vibrational frequencies together with IR, Raman, and VCD intensities including both mechanic and electric anharmonicities have been recently reviewed and we make reference to those studies for these aspects[15, 16]. On the other hand, an integrated time dependent and time independent approach to vibronic spectroscopies is less documented (actually completely new for CPL) and we give in the following a sketch of the most significant aspects.

2.1.1 General theory of vibronic spectroscopy

We recall here the sum-over-states expression for a one-photon vibronic spectrum, adopting the general formulation proposed previously to facilitate the extension of our procedure to new spectroscopies[16, 17, 19]

$$I = \alpha\omega^{\beta}\sum_m\sum_n \rho_\gamma \mathbf{d}^{A}_{mn}\mathbf{d}^{B}_{mn}{}^{*}\delta\left(\frac{E_n - E_m}{\hbar} - \omega\right) \quad (1)$$

where ω is the incident frequency (in Hz) and ρ_γ is the Boltzmann population of the molecular state γ. One-photon absorption and emission spectroscopies can be easily included in this formulation together with electric circular dichroism by defining the parameters α, β and γ, as well as the transition dipole moments, $\mathbf{d}^{A}_{mn}$ and $\mathbf{d}^{B}_{mn}$, in the proper way. The following equivalency table (in SI units) summarizes the values of each parameter for each type of spectroscopy,

Type	I	α	β	γ	$\mathbf{d}^{A}_{mn}$	$\mathbf{d}^{B}_{mn}$
OPA	ε(ω)	$10\pi\mathcal{N}_A/\left[3\epsilon_0 \ln(10)\hbar c\right]$	1	m	$\boldsymbol{\mu}_{mn}$	$\boldsymbol{\mu}_{mn}$
OPE	I_{em}/N	$2\mathcal{N}_A/\left[3\epsilon_0 c^3\right]$	4	n	$\boldsymbol{\mu}_{mn}$	$\boldsymbol{\mu}_{mn}$
ECD	Δε(ω)	$40\pi\mathcal{N}_A/\left[3\epsilon_0 \ln(10)\hbar c^2\right]$	1	m	$\boldsymbol{\mu}_{mn}$	$\Im(\mathbf{m}_{mn})$

where ε(ω) is the molar absorption coefficient for a given angular frequency ω (in $dm^3\ mol^{-1}\ cm^{-1}$), Δε(ω) (in $dm^3\ mol^{-1}\ cm^{-1}$) is the difference (referred to as anisotropy) between the molar absorption coefficients $\varepsilon^{-}(\omega)$ and $\varepsilon^{+}(\omega)$ relative to the left and right circularly polarized light, respectively, and I_{em}/N is the energy emitted by one mole per second (in $\mu J\ mol^{-1}\ s^{-1}$).

$\mathbf{d}^{A}_{mn}$ and $\mathbf{d}^{B}_{mn}$ are respectively the transition moments of $\mathbf{d}^{A}$ and $\mathbf{d}^{B}$ between the lower (Ψ_m) and higher (Ψ_n) total molecular states,

$$\mathbf{d}^{X}_{mn} = \langle \Psi_m | \mathbf{d}^{X} | \Psi_n \rangle$$

where "X" represents either "A" or "B".

In this general and flexible framework, addition of circularly polarized luminescence (CPL) has been greatly facilitated. In CPL spectroscopy the sample is irradiated with a non-polarized light and the difference between the number of emitted photons with left-handed polarization and those with right-handed polarization is measured. The theoretical foundation of CPL spectroscopy has been widely discussed[21-27]. Emeis and co-workers, in their pioneering papers, established that both ECD and CPL transitions depend on the rotational strength, which is defined as $R_{mn} = \boldsymbol{\mu}_{mn} \cdot \Im(\mathbf{m}_{nm})$ [23, 25]. However, a more rigorous derivation has been given by Riehl and Richardson, based on quantum electrodynamic theory[24, 26]. Following this approach, it is possible to derive an analytical expression for the intensity of a CPL transition:

$$\Delta I_{em}/\mathrm{N} = \frac{8\omega^4}{3\epsilon_0 c^4}\sum_m\sum_n \rho_n \Im\left(\boldsymbol{\mu}_{mn}\cdot\mathbf{m}_{nm}\right)\delta\left(\frac{E_n - E_m}{\hbar} - \omega\right) \quad (2)$$

By comparing eqs. (2) with (1), we obtain the following set of parameters to be used in the general formulation,

Type	I	α	β	γ	$\mathbf{d}^{A}_{mn}$	$\mathbf{d}^{B}_{mn}$
CPL	$\Delta I_{em}/N$	$8\mathcal{N}_A/\left[3\epsilon_0 c^4\right]$	4	n	$\boldsymbol{\mu}_{mn}$	$\mathfrak{I}(\mathbf{m}_{mn})$

In practice, to compute the transition intensities, the Born-Oppenheimer and Eckart conditions are used, so that the transition dipole moment $\mathbf{d}^{X}_{mn}$ can be rewritten,

$$\mathbf{d}^{X}_{mn} = \langle \chi_{r(\underline{m})} | \mathbf{d}^{X}_{e,mn} | \chi_{s(\underline{n})} \rangle \tag{3}$$

where $\chi_{r(\underline{m})}$ represents the vibrational wave function associated to the vibrational state r and the electronic state $\underline{m}$ for the total lower molecular state m, and $\chi_{s(\underline{n})}$ its counterpart for the total higher molecular state n

However, analytical expressions for the electric dipole transition moment are not known, thus equation (3) must be further simplified. A Taylor expansion of the transition dipole moment with respect to the normal modes **Q** around the equilibrium geometry of one of the electronic states is usually employed:

$$\mathbf{d}^{X}_{mn}(\mathbf{Q}) = \mathbf{d}^{X}_{mn}(\mathbf{Q}_{eq}) + \sum_{i=1}^{N} \left.\frac{\partial \mathbf{d}^{X}_{mn}}{\partial Q_i}\right|_{eq} Q_i + \ldots \tag{4}$$

The zeroth order term corresponds to the well-known Franck-Condon (FC) approximation[28-31], which assumes that the electronic transition happens in such a short time that the nuclei remain in their equilibrium positions. This approximation is satisfactory for strongly-allowed transition and when the potential energy surfaces (PES) of the ground and excited states are similar. However, when those conditions are not met, the inclusion of the linear terms in the Taylor series (first order in eq. (4)), namely the Herzberg-Teller (HT) approximation[32], is mandatory. Moreover, for ECD and CPL spectroscopy, the Franck-Condon approximation is generally poorly suited because the electric transition dipole moment and the magnetic one can be near-orthogonal, resulting in a small FC contribution to the vibronic spectrum insufficient to correctly reproduce the experimental spectrum. The limitations of the FC approximation are even more tangible when the band-shapes of ECD or CPL spectra show an alternation of sign, which cannot be reproduced at the FC level[33].

Finally, the calculation of the matrix elements of the electric dipole moment operator requires a relation between the normal modes of the lower and higher states. In the following, we will use the Duschinsky transformation[34], which assumes a linear relation between the two sets of normal modes. This approximation has been shown to give satisfactory results for semi-rigid molecules.

$$\mathbf{Q}_m = \mathbf{J}\mathbf{Q}_n + \mathbf{K}$$

2.1.2 From the time-independent to the time-dependent formulation

By inserting the Taylor expansion given in eq. (4) in eq. (1), the calculation of the transition intensities can be done and the generation of the band-shape becomes straightforward. Within the harmonic approximation, the most effective and general approach to compute the resulting integrals $\langle \chi_{r(\underline{m})} | \chi_{s(\underline{n})} \rangle$ relies on recursive formulae[35, 36], which require only the overlap integral between the vibrational ground states of the initial and final electronic states to be known analytically. A remaining problem is the infinite summation of transition integrals, most of which are negligible. In order to make time-independent calculations

computationally affordable, the use of a prescreening scheme in order to identify *a priori* and compute only the most intense transitions is needed (see refs [17, 19, 37-40] for more details on the prescreening models). Since not all transitions are accounted for, the quality and reliability of the prescreening needs to be assessed by comparing the calculated intensity with the analytic one obtained by mean of the analytic sum rules.

Conversely, the problem of the infinite summation can be overcome by rewriting eq. (1) in a time-dependent formulation. The basic idea is to switch from the frequency domain to the time domain by exploiting the properties of the Fourier transform of the delta function. After some mathematical manipulation, the general experimental observable can be rewritten as the Fourier Transform of a time-dependent function, the transition dipole moment autocorrelation function,

$$I = \frac{\alpha\omega^{\beta}}{Z}\int_{-\infty}^{+\infty} dt\ \mathrm{Tr}\left(\mathbf{d}^{\mathrm{A}}_{e,mn} e^{-\hat{H}_n\tau_n}\mathbf{d}^{\mathrm{B}}_{e,mn}{}^{*} e^{-\hat{H}_m\tau_m}\right)e^{i(\omega_{\mathrm{ad}}-\omega)t}$$

where Z is the canonical partition function of the vibrational levels of the initial state, ω_{ad} is the difference of energy between the two minima of the PES, $\hat{H}_m$ and $\hat{H}_n$ are the vibrational hamiltonians of the lower and upper states, respectively and τ_m and τ_n are auxiliary variables, which include both time and temperature, defined as follows,

	τ_m	τ_n
Absorption	$\frac{1}{k_B T} - \frac{it}{\hbar}$	$\frac{it}{\hbar}$
Emission	$-\frac{it}{\hbar}$	$\frac{1}{k_B T} + \frac{it}{\hbar}$

The time-dependent theory provides a link between vibronic spectroscopy and dynamics. Indeed, the autocorrelation function can be obtained by propagating the initial state wavefunction over the PES of the excited state. In this framework, the transition dipole moment integral is calculated analytically during the propagation by assuming that both the PESs *and property surface (PS)* are harmonic. It is noteworthy that our implementation takes into account mode mixing and Herzberg-Teller effects as well (see Ref. [18] for details on the implementation). In practice, the vibronic spectrum can be obtained by sampling the autocorrelation function and computing numerically the integral with a discrete Fourier transform algorithm.

Let us finally point out that the time-dependent and time-independent approaches should be regarded as complementary techniques. Indeed, the application of both provides a more extensive description of the simulated spectrum. Thanks to the automatic inclusion of all vibronic transitions, the time-dependent approach gives a general picture of the spectrum band-shape. Moreover, temperature effects can be straightforwardly accounted for with no consequence on the computational cost. As the time-independent approach can become quickly expensive if a large number of vibronic initial states must be included in the calculations, it is interesting to first check the impact of temperature on the spectrum. From the sum-over-states formulation, the contribution of each transition to the overall band-shape can be known and the observed bands can be assigned to the proper transition or set of transitions. From a technical point of view, performing spectrum simulations with both time-dependent and time-independent approaches offers the possibility to control the numerical stability of the former and the band-shape convergence of the latter.

2.1.3 Inclusion of anharmonicity

The theoretical framework presented up to now is based on the assumption that both the PESs are harmonic and the property surfaces (PSs) are linear in the neighborhood of the equilibrium structures. In order to get a more accurate description of the vibrationally-resolved electronic spectra, it is necessary to go beyond the harmonic approximation. However, a full anharmonic calculation of transition intensities becomes quickly prohibitive and must be limited to small systems[41-45]. An alternative approach to include anharmonic corrections at a lower computational cost is to replace the harmonic frequencies with their anharmonic counterparts, while keeping the equations used to compute the intensities unchanged so there is no increase of computer time in the generation of vibronic spectra.

Several approaches have been proposed to compute vibrational energies beyond the harmonic level of theory. While the most accurate models are able to provide an accurate representation of the PES to obtain converged vibro-rotational levels[46-52], for medium-to-large systems, approximations are needed to make anharmonic calculations computationally feasible. Apart from improved empirical procedures based on transferable scaling factors in internal coordinates, the most successful methods are based on the vibrational self-consistent field (VSCF) [53-61] or VPT2[62-70][71-75]. The VPT2 approach is particularly appealing as it can provide accurate results at a reasonable computational price. In this work, the generalized VPT2 (GVPT2) model was used to overcome the problem of singularities due to the presence of Fermi resonances. Terms defined as resonant by mean of *ad hoc* criteria are removed in the VPT2 expansion and then treated variationally in a second step (see ref. [70, 76, 77] for more details on the protocol).

The calculation of anharmonic vibrational energies at the VPT2 level requires third and semi-diagonal quartic force constants, which are generally obtained by mean of numerical differentiation of analytic harmonic force constants. While this is now routinely feasible at the DFT level, this task is complicated at the TD-DFT level for two reasons. First, most electronic structure computational programs only have analytic gradients and already the harmonic force constants are computed by differentiating numerically the gradients, so that cubic and quartic terms cannot be estimated by one-dimensional finite differences. Second, the computational cost of frequency calculations at the TD-DFT level is high, the more so to obtain the full set of third and semi-diagonal force constants. An alternative way is to estimate the anharmonic frequencies of the excited state from those of the ground one by applying a mode-specific scaling scheme, as proposed by our group[78]. Indeed, if there are significant changes between the PESs of the two electronic states, the anharmonic correction of the frequencies of the ground state cannot be simply applied to those of the excited one. However, the Duschinsky transformation can be used in order to calculate a scaling factor for the frequencies of the excited state using the following relation,

$$\nu''_a = \left[\sum_b \mathrm{J}_{ab}{}^2 \frac{\nu'_b}{\omega'_b} \right] \times \omega''_a \qquad (5)$$

where ω and ν are the harmonic and anharmonic frequencies, respectively, and J_{ab} is an element of the Duschinsky matrix. The prime and double prime symbols represent the lower and higher electronic state, respectively.

It should be noted that the range of application of the previous equation goes beyond the inclusion of anharmonic effects. Indeed, it can also be used between two sets of harmonic frequencies but calculated at different levels of theory. In this case, the two methods of interest, one of which being more accurate but more computationally expensive, are applied to the ground state. Then, equation (5) can be used to extrapolate the excited state's frequencies with the more accurate model from those of the lower-level one.

2.1.4 Inclusion of environment effects

Vibronic spectra are usually recorded in solution, especially for medium- and large-size molecules. Therefore, in order for the theoretical spectra to be comparable to experiment, environmental effects must be included. Indeed, solvent effects may result in substantial changes in the structures and the PESs of both ground and excited state and consequently on the simulated vibronic spectra, with shifts in the band positions and variations of the peak intensities.

Since the solvents considered in this work do not have specific interactions with the solute, such as forming hydrogen bonds, the Polarizable Continuum Model (PCM)[10] has been used to include solvent effects in QM calculations. In PCM, the solvent is treated as a continuum polarizable dielectric medium characterized by a dielectric constant. The solute molecule, treated quantum mechanically, is accommodated within a molecule-shaped cavity. The presence of the polarizable continuum alters the solute electronic density, via an effective solvent-dependent term in the molecular Hamiltonian, which in turn affects the solvent response, until self-consistency, which results in mutual solute-solvent polarization effects.

To simulate absorption phenomena, calculations in the ground electronic state are carried out assuming that all the degrees of freedom of the solvent are equilibrated with the electronic density of the solute (equilibrium regime). However, this approach cannot be applied to calculations in excited states. Indeed, light absorption is a dynamical process and the response of the solvent will take place at different timescales. For one-photon vibronic spectroscopy, the most common approximation is to assume that the electronic degrees of freedom of the solvent quickly adapt to the evolving solute electronic density, while the rest remains equilibrated with the ground-state density. As a consequence, we will assume a non-equilibrium regime for the excited state[20].

Finally, it should be noted that solvent has a broadening effect on the peaks in a vibronic spectrum. In our simulations, this is accounted for by applying Gaussian distribution functions with half-width at half-maximum set to match the experimental spectra.

2.2 Computational details

All calculations were performed with a development version of the GAUSSIAN suite of quantum chemical programs[79] using the density functional theory (DFT) for the ground states and its time-dependent extension (TD-DFT) for excited states. Except where specified otherwise, the B3LYP functional[80] was used together with the polarized double-ζ SNSD basis set[81], which has been developed in our group to provide good results at a limited computational cost for spectroscopic studies of medium-to-large systems. This basis set has been built from the N07D basis set[82-85] by consistently including diffuse *s* functions on all atoms, and one set of diffuse polarized functions (*d* on heavy atoms and *p* on hydrogens). Solvent effects were accounted for by mean of the integral equation formalism for the polarizable continuum model (IEF-PCM)[86] and the solute cavity was built with the default parameters, that is by using a set of interlocking spheres centered on the atoms with the following radii (in Å): 1.443 for hydrogen, 1.926 for carbon, and 1.750 for oxygen, each multiplied by a factor of 1.1. The solvents' static and optical dielectric used are $\varepsilon = 2.23$ and $\varepsilon_{opt} = 2.13$ for CCl_4 and $\varepsilon = 2.02$ and $\varepsilon_{opt} = 2.04$ for cyclohexane.

Geometry optimizations were performed with tight convergence criteria (convergence on force: 10^{-5} Hartree/Bohr, Convergence on estimated displacement: $4 \cdot 10^{-5}$ Bohr). As a reminder, TD-DFT harmonic frequencies and DFT cubic and quartic force constants are generated internally in GAUSSIAN by numerical differentiations. The former are obtained from the analytic gradients by displacing each atom along a single Cartesian coordinate (step: $\delta x = 10^{-3}$ Å) at a time. The latter are calculated from the harmonic force constants by shifting the atom positions along the mass-weighted normal coordinates (step: $\delta Q = 10^{-2}$ amu$^{1/2}$·Å).

Let us recall that, in order to minimize vibration-rotation couplings, the Eckart orientation is used for the electronic ground state and, for adiabatic models, a maximum superposition algorithm is employed to align ground- and excited-state structures[87, 88].

For vibronic calculations, the computational protocol to be used depends partially on the chosen model. For the initial state, the procedure remains identical with harmonic frequencies computed at the equilibrium geometry. For the final state, data to be computed vary. For adiabatic hessian (AH), both PESs are treated at the same level, so the harmonic frequencies in the final state are calculated at its equilibrium geometry. Adiabatic shift (AS) is a simplification of AH where both PES are assumed to be equal, only shifted, so only geometry optimization needs to be carried out in the final state. Finally, vertical gradient (VG, also known as Linear Coupling Model[89]) is an approximated approach based on a slightly different model, called vertical hessian (VH). Since both initial and final PESs are calculated about their respective minima, AH generally provides an equilibrated description of the vibronic spectra with an overall good description of the fine structure. However, if the PESs are shifted, the description of the PES of the final state in the Franck-Condon region can be insufficient, leading to approximations of the most intense bands. Conversely, the PES of the final state in the VH model is calculated about the equilibrium geometry of the initial state, so the most intense region of the spectrum is generally reproduced better than with AH, at the expense of a less accurate fine structure. Similarly to AS, the PESs are assumed to be the same in the VG model, so only the potential energy gradient of the final state at the equilibrium geometry of the initial one needs to be computed to extrapolate the shift of the final state's PES (see Ref.[39] for details). For simulations with the time-independent approach, transitions from the ground state to states with up to 7 simultaneously excited oscillators were considered. Transitions are grouped in classes based on the number of modes with non-null quanta in the final state. Classes 1 (overtones) and 2 (combination bands of two modes) are treated up to a set number of quanta (C_1^{max}=20 for class 1 and C_2^{max}=13 for each mode in class 2). For class 3 and above, a class-based prescreening[17, 19, 37-40] is used to choose *a priori* the most intense transitions, taking at most 10^8 integrals per class. For the time-dependent approach, the total time used for the simulation was 10^{-9} s discretized in 2^{24} steps. Convergence of the Fourier transform was ensured by a mean of a rectangular window function spanning over 2^{16} points (the value of the autocorrelation function was kept untouched over 2^{16} points and forced to be null over the tailing "2^{24}-2^{16}" steps of the discretization).

For vibrational spectra, absolute intensities and frequencies were used to compare theoretical results with their experimental data. For vibronic spectra, such a strategy is often not viable when the band-shapes are to be examined. Indeed, calculated energies between the electronic states are often approximated, with the first noticeable impact being a shift of the band-shapes with respect to experimental spectra. As a consequence, the spectra are generally plotted in relative energies with respect to their relative 0-0 transition (between the vibrational ground states of each electronic state). Since this error also influences the intensities, the spectra must be generally normalized so that their respective highest bands have an arbitrary intensity of 1, for instance.

The computational protocol followed here has been systemized from frequent usage and can be adapted based on the following observations:

- For organic systems, the combination B3LYP/SNSD has been shown to provide reliable results at a reasonable computational cost for vibrational and vibronic studies. If charge transfer is present, the CAM-B3LYP[90] and M06-2X[91] exchange-correlation functionals are to be used to obtain correct energies for the electronic transition while the frequencies can be calculated at the usual B3LYP/SNSD level. For dimers, the semi-empirical extension "DFT-D3"[92, 93] can be used. Since the additional cost it induces is small, it can be used to compute frequencies as well.

- Vibrational energies, both at the harmonic and anharmonic levels are now easily accessible. Extended benchmarks have provided data to find reliable default settings so anharmonic calculations at the VPT2 level (in particular the deperturbed and generalized approaches) can be routinely done in a black-box procedure and give accurate values even in the presence of Fermi resonances. Nevertheless, a resonance-free treatment is possible at the hybrid degeneracy-corrected VPT2 (HDCPT2) level with very low impact on the accuracy of the resulting frequencies.
- As less work has been dedicated to anharmonic IR and VCD intensities especially concerning the problem of resonances, the definition of a robust and general treatment of this problem is still under investigation. The effectiveness of the deperturbed treatment, currently used in Gaussian, should be assessed from IR intensity calculations first as the sign alternation present in VCD spectra associated to low-intensity bands may result in error corrections, which make more difficult the identification of excessive contributions due to resonances.
- Regarding vibronic spectroscopy, default parameters for the time-independent approach have been carefully tailored so that most simulations –within the boundaries of the theoretical framework described previously, that is a semi-rigid system with limited change in the positions of the nuclei during the electronic transitions- can be done with no additional settings from the user. If the mode-mixing is high, complete or near-complete convergence of the spectrum may require increasing the parameters used by the prescreening algorithm (namely C_1^{max}, C_2^{max} and the maximum number of integrals per class). As noted before, the time-dependent approach may suffer in some cases of numerical instability. This is often related to artefacts present in the discrete integral of the autocorrelation function, which may give further oscillations to the final band-shape. The presence of a default window function limits this phenomenon to a minimum. If a higher resolution of the band-shape is desired (with low broadening), a correct simulation may require a finer graining, that is more discretization steps, and an adaptation of the window function to the number of points used to compute the autocorrelation function (in general, it is sufficient to keep the ratio between the window function and the total number of steps constant). An alternative way, currently under investigation, would be the use of more complex window functions.

3 Results and Discussions

The points discussed above will be illustrated in the following by means of three case studies starting from vibrational spectra and proceeding toward increasingly complex vibronic spectra.

3.1 (1S,4S)-bicyclo[2,2,2]octan-2,5-dione

As a first application of our virtual spectrometer we consider vibrational spectroscopy beyond the harmonic level of approximation. Indeed, an extensive characterization of chiroptical molecules will generally involve multiple, complementary spectroscopies. Vibrational spectroscopy can now be routinely simulated with a wide range of computational packages, but this is often done at the harmonic level. A further refinement consists in correcting the band position by using anharmonic frequencies, but this does not solve the issue that only fundamental bands will have non-vanishing intensities. This shortcoming can be overcome by including anharmonic effects into intensities as well. We have used here the procedure described in Ref. [14] to compute the IR and VCD spectra of (1S,4S)-bicyclo[2,2,2]octan-2,5-dione (molecule 3 in Fig. 1) and compared them to the experimental ones shown in Ref. [94]. To match experimental conditions, solvent effects (CCl_4) were simulated with IEF-PCM. While not a large molecule, (1S,4S)-bicyclo[2,2,2]octan-2,5-dione can represent a somewhat challenging task to obtain anharmonic data at a high level of theory. For this reason, B3LYP/SNSD was used here to generate the data needed for the anharmonic frequencies (third and semi-diagonal fourth derivatives of the potential energy) and transition moments (second and semi-diagonal

third derivatives of the electric and magnetic dipole moments). Several studies have shown that anharmonic and bulk solvent effects are accurately reproduced by PCM/B3LYP/SNSD computations, whereas the underlying harmonic frequencies can be improved by coupled-cluster models (CCSD(T)) or double hybrid (especially B2PLYP) functionals[95] employing basis sets of at least cc-pVTZ quality. Here we have followed this hybrid approach based on the assumption that the various contributions (solvent effects, use of more accurate methods…) were additive[96-101][102]. This allows a fine-tuning of different contributions depending on computer time and/or availability in different packages (for instance missing solvent models). The harmonic frequencies used for our calculations (ω_{best}) were obtained from the following relation,

$$\omega_{best} = \omega_{B3LYP}^{vac} + \Delta_{PCM} + \Delta_{B2PLYP} \quad (6)$$

with

$$\Delta_{PCM} = \omega_{B3LYP}^{PCM} - \omega_{B3LYP}^{vac}$$
$$\Delta_{B2PLYP} = \omega_{B2PLYP}^{vac} - \omega_{B3LYP}^{vac}$$

where ω_{B3LYP}^{PCM} and ω_{B3LYP}^{vac} are the harmonic frequencies calculated at the B3LYP/SNSD level in solvent and vacuum, respectively, and ω_{B2PLYP}^{vac} are the harmonic frequencies calculated at the B2PLYP/cc-pVTZ level in vacuum. Band broadening was simulated with Lorentzian functions with half-width at half-maximum of 5 cm^{-1}.

The IR and VCD spectra are reported in Figs. 2 and 4, respectively. As expected, harmonic frequencies are systematically overestimated while agreement with experiment becomes very good once anharmonic effects are included. For band intensities, the results are more mitigated. If we discard the band shift of the harmonic spectrum, we note for the IR spectrum (Fig. 2) that it reproduces better the relative intensities of the four main peaks than the anharmonic one. Indeed, it appears that inclusion of anharmonic effects causes an increase of the intensity of the highest band and a decrease of the three other ones' intensities. Consequently, while still visible, the strongest bands are systematically lower with respect to the highest one than in the experimental spectrum. This observation changes once we focus on the low-intensity features of the band-shape. At this level of detail, the anharmonic spectrum shows a better agreement. For instance, the harmonic spectrum shows a spurius peak on the left of the most-intense band, which is more correctly represented as a shoulder in the anharmonic spectrum in a way similar to the experimental one. Conversely, a peak is missing in the harmonic spectrum at about 1305 cm^{-1} in the experimental spectrum, which is assigned in the anharmonic spectrum to a combination band ($|8^1 16^1\rangle$, see Fig. 3 for a representation of those modes). On the whole, anharmonic calculations are able to capture most features of the spectrum and permit an extensive assignment of the peaks observed experimentally. At variance with the IR spectrum, the anharmonic VCD spectrum (Fig. 4) shows a more balanced band-shape with a better estimation of the most intense transitions. The overall band-shape is quite satisfactory, even if some marked discrepancies can be observed in particular in the 1200–1300 cm^{-1} region. As a concluding note, we would like to highlight that this molecule represents a challenging system for anharmonic calculations due to the presence in the region of interest of accidental degeneracies (and the risk of 1-1 resonances, $\omega_i \approx \omega_j$, in the calculation of the intensities of fundamental bands) and Fermi resonances (which are present in the transition moment integrals of fundamental, overtones and combination bands). While the procedure is able to identify and remove such singularities in intensity calculations, which would result in excessive anharmonic contributions, the current implementation does not include yet a successive step to reintroduce the missing terms as done with the variational correction for the frequencies. This limitation is likely to have an impact on the resulting band-shape reported here. In any case, the functional (B3LYP), basis set

(SNSD), and anharmonic model (VPT2) appear largely sufficient for the description of vibrational signatures especially for the smearing (possibly non symmetric) effects on electronic spectra unless extremely high resolution experiments are considered.

3.2 ECD spectrum of (2R,3R)–dimethyloxirane

Thanks to their small size (2R,3R)-trans-dimethyloxirane (molecule 1 in Fig. 1) and (2S,3S)-trans-dimethyloxirane represent interesting prototypical molecules to test theoretical and computational models on optically active systems[4, 103-109][3, 18]. More specifically, the availability of experimental ECD data spanning several electronic transitions[110] and the clear evidence of a visible vibronic structure in the recorded spectrum are particularly adequate for validating electronic structure protocols[3, 4, 104-107, 111] and programs or modules designed to simulate vibrationally resolved electronic spectra[18, 108, 109]. However, the Rydberg and charge transfer character of the lower electronic states and the presence of conical intersections make dimethyloxirane doubly challenging. It is not trivial to get the correct layout of excited states from electronic structure calculations and to get the correct vibronic structure by choosing the most relevant models for the simulation of the overall ECD spectrum. In this study, we will limit our analysis to the electronic transitions from the ground state to the first 4 excited states, which correspond to the 6.8–7.8 eV region of the experimental spectrum given in Ref. [110]. As shown in Ref. [111], these transitions are respectively $n \rightarrow 3s$ for the first transition followed by 3 transitions of character $n \rightarrow 3p$. Similarly to what has been done before[108, 109], the transition energies have been corrected to match experimental data, here using values from multi-reference configuration interaction (MRCI) calculations[111]. Finally, the experimental spectrum was shifted by -3000 cm^{-1} to match the positions of the first bands of the experimental and simulated spectra. We have adopted here the protocol presented by Neugebauer *et al.*[108] to simulate the overall ECD spectrum, using the vertical gradient model at the Franck-Condon level (VG|FC). Gaussian distribution functions with full-width at half-maximum of 300 cm^{-1} were used to simulate the band broadening. To get a comprehensive picture of the ECD spectrum, both TI and TD approaches were used to simulate the overall spectrum and to gain information on the various contributions to the band-shape. The resulting spectra are shown in Fig. 5. The first spectrum was simulated at T=0K and with harmonic frequencies (VG|FC) as usually done in most computational protocols and in Ref. [108] as well. The first negative band of the experimental spectrum, which corresponds to the $S_1 \leftarrow S_0$ transition is in fair agreement with experiment. However, the rotatory strength of the second electronic transitions appears overestimated, resulting in a series of strong positive bands absent in the experimental spectrum. Such an observation is in line with previous analyses[104, 111]. This has also an impact on the second series of negative bands after 57000 cm^{-1}, as it partially cancels the contributions from the third transition and only the higher-energy region, above 59000 cm^{-1}, is correctly reproduced. In a successive step, the harmonic frequencies of the ground state were replaced with their anharmonic counterparts, and the mode-specific scaling scheme described before was used to correct those of the excited state (VG|FC anharm). A general improvement of the band-shape can be observed with a good reproduction of the first negative band. The intensity of the $S_2 \leftarrow S_0$ transition is still overestimated but an improvement can be observed with less intense positive bands. On the whole, the band-shape related to this transition seems globally shifted toward negative intensities. As a direct consequence, the beginning of the second experimental negative band at 57500 cm^{-1} is now qualitatively reproduced but the higher region is now slightly overestimated. Finally, adding temperature effects to the previous simulation (VG|FC T=298 K anharm) further alters the theoretical spectrum. The first block of negative bands remains correctly reproduced even if the separation between the two bands becomes deeper, at variance with the experimental spectrum. For the second transition, no improvements are visible, with only slightly stronger negative bands. However, the second series of negative bands in the experimental spectrum is reproduced better with the simulated bands closely matching the height of the experimental feature. As a last remark of this analysis, while the inclusion of anharmonic and temperature effects clearly improves the

agreement with experimental data, use of more accurate methods to perform electronic structure calculations is needed in order to obtain the correct contribution of each electronic transition when simulating spectra spanning several transitions. As a concluding remark, it has been suggested in Ref. [109] that the relative intensities of the various electronic bands are affected by non-adiabatic couplings. it may be possible to model this by HT effects, but some normal modes (asymmetric) may require quadratic contributions.

To illustrate the influence of various computational models on the resulting vibronic spectra, we focus on the ECD spectrum corresponding to the first electronic transition ($S_1 \leftarrow S_0$). Such a comparison is important in order to assess the reliability of approximated models. Band broadening was obtained with Gaussian distribution functions with half-width at half-maximum of 300 cm^{-1}. The various spectra are gathered in Fig. 6. Among the considered models, AH|FCHT is the most accurate one. Analysis of the stick spectrum shows some predominant transitions contributing mainly to the band-shape. The first band is mostly related to the transition between the vibrational ground states while the second one is the contribution of two fundamentals ($|0\rangle \rightarrow |14^1\rangle$ and $|0\rangle \rightarrow |16^1\rangle$; modes 14 and 16 are represented in Fig. 7). Finally, the third band involves a multitude of low-intensity bands with the highest contribution being a combination band ($|0\rangle \rightarrow |14^1 16^1\rangle$). Inclusion of anharmonic corrections (AH|FCHT anharm) using the mode-specific scaling scheme presented before has very little impact on the band-shape, so anharmonicity can be safely disregarded in this case. Similarly, Herzberg-Teller effects are small as the band shape simulated with AH|FC is mostly superimposed with the reference one (AH|FCHT), the only noticeable difference being a slight increase in the intensity of the second band. This is expected since the AH|FCHT stick spectrum only showed peaks of the same sign, hinting at a low contribution from the Herzberg-Teller terms. The two remaining models, namely AS|FC and VG|FC, assume that both PESs are equal. As a first consequence, the difference between the zero-point vibrational energies (ZPVE) of the initial and final states obviously vanishes, which explains the general shift observed with respect to the adiabatic hessian band-shapes. To improve the readability of the figure, the sign of AS|FC and VG|FC band-shapes was inverted (they are negative by default). The main difference between AS|FC and VG|FC lies in the shift vector. In the former model, the equilibrium geometry of the final state is known, so the shift vector can be calculated without any further approximation with respect to AH, while for the latter one, it is extrapolated from the energy gradient of the final state, assuming that the PES is harmonic and equal to that of the initial state. Since the shift vector is small for this transition, the extrapolation of the minimum of the final-state PES is rather good, as shown by the near superposition of the first band of AS|FC and VG|FC. However, stronger discrepancies arise at higher energies with a small shift of the second and third band and a noticeable difference of intensities. As a consequence, the analysis of the ECD spectrum of dimethyloxirane with a higher resolution could be prone to errors if carried out at the VG|FC level. Finally, the impact of the approximation from the assumption that both PESs are equal can be estimated by comparing the band-shapes calculated with AS|FC and AH|FC. To simplify this analysis, the AH|FC band-shape was shifted (AH|FC shifted) in order to superpose the first band of AH|FC and AS|FC, which correspond to assuming that the difference between the ZPVEs is null. The band-shapes are rather similar, the main impact of neglecting mode mixing being that the second and third bands appear narrower than with AH|FC. This difference is mostly due to the absence of low-intensity transitions in the AS|FC spectrum.

3.3 ECD and CPL spectra of (1R)-camphorquinone

As an example of the applicability of our procedure to larger systems, we have simulated the vibrationally-resolved ECD ($S_1 \leftarrow S_0$) and CPL ($S_1 \rightarrow S_0$) spectra of (1*R*)-camphorquinone ((1*R*,4*S*)-1,7,7-trimethylbicyclo[2,2,1]heptane-2,3-dione, shown in Fig. 1), which has been recently investigated by Longhi and coworkers[94]. To match experimental conditions, solvent effects (CCl_4 for ECD and cyclohexane for CPL) were accounted for by using the polarizable continuum model and Gaussian distribution functions with

half-width at half-maximum of 350 cm^{-1} were used to broaden the theoretical band-shape. The time-independent version of the Adiabatic Hessian model was employed to simulate the spectra. As shown in Fig. 8, the change in geometry related to the electronic transition is small (right panel). More meaningful information is given by plotting the shift vector (left panel), which shows the geometric displacement projected on the mass-weighted coordinates of the initial electronic state. Indeed, in case of difficulty to reach a good convergence with the time-independent approach, such a graph gives the possibility to identify straightforwardly modes highly shifted so that corrective solutions can be devised, such as increasing the number of quanta in the simulation (C_1^{max} and C_2^{max}) or using a block model where problematic modes are handled separately at a higher level of theory for instance.

The $S_1 \leftarrow S_0$ ECD spectra corresponding to the HOMO-LUMO transition (see Fig. 9 for plots of frontier molecular orbitals) are gathered in Fig. 10. Since the experimental spectrum shows no sign change, the Franck-Condon approximation (AH|FC) may be sufficient to obtain a qualitative agreement with reference data, even without taking into account solvent effects. The experimental spectrum has a broad shape with a clear band, which corresponds to the transition between the vibrational ground states (0-0 transition), and some vibronic features appearing as shoulders on the right side, at higher energy. Two shoulders are distinguishable, at about 500 and 1250 cm^{-1} with respect to the 0-0 transition and a last band can be guessed at about 2100 cm^{-1}. These bands are also visible in the AH|FC spectrum but seem shifted to higher energies (at about 800, 1450 and 2400 cm^{-1}, respectively) and overestimated. By adding the Herzberg-Teller effect (AH|FCHT) in the simulation, we note a change in the shape with an overall decrease of the intensity of the band-shape at higher energy. The agreement with experiment in the band position is improved and the tail of the spectrum at higher energy is well reproduced, but the first two bands are now underestimated. Including solvent effects with PCM (the solvent was chosen to be the same as Ref. [94]) corrects the intensity of those two bands but they remain lower than the registered ones. The changes between AH|FC and AH|FCHT can be explained by the stick spectrum issuing from AH|FCHT approach. Indeed, the latter shows an alternation of positive and negative signs, while the AH|FC model can only show peaks of a unique sing. When broadening functions are applied, the sign change will have a damping effect on the AH|FCHT band-shape, which explains the overall decrease of intensities. Overtones of modes 18, 19 and 20, which are represented in Fig. 11 with their associated wavenumbers, give the highest contributions to the spectrum.

For the CPL spectrum (Fig. 12), experimental data were taken from Ref. [27] since the experimental spectrum in Ref. [94] was showing a strong noise due to the weakness of the signal, which did not allow the clear identification of vibronic features in the spectrum. While the ECD spectra published by Luk and Richardson[27] and Longhi *et al.*[94] were similar, the difference of resolution in their reported CPL spectra makes the identification of a vibronic structure more equivocal. The solvent used in Ref. [27] was cyclohexane, so the latter was used for the simulation with solvent effects. Noticeable differences in the simulated band-shape with respect to ECD appear. The first one is that AH|FC has now a lower intensity with respect to AH|FCHT. However, in the same way as before, solvent effects are low and result in a slight increase of intensity in the left-wing of the band-shape. This time, all theoretical spectra are below the experimental one. At variance with the ECD spectrum, a second vibronic band appears more distinctively in CPL, even if again as a shoulder of the single, broad band. This seems better reproduced by taking into account Herzberg-Teller effects, even if a strong shift of about 260 cm^{-1} is observed. The CPL stick spectrum shows noticeable differences with respect to its ECD counterpart. First of all, more intense transitions can be observed with respect to the latter. A first consequence is that the bands obtained by applying broad distribution functions will be the result of several important contributions, causing energy shift of their maximum. For instance, the first band, which was unambiguous in ECD and assigned to the 0-0 transition is here the sum of at least two major transitions, the transition between the vibrational ground state and the transition from the

ground state to the single overtone $|2^1\rangle$. Similarly, three transitions contribute predominantly to the second band (respectively $|0\rangle \rightarrow |24^1\rangle$, $|0\rangle \rightarrow |31^1\rangle$ and $|0\rangle \rightarrow |2^1 31^1\rangle$ starting from the right). The modes, which contribute to the main bands are represented in Fig. 13. As with ECD, the AH|FCHT stick spectrum shows peaks of both positive and negative signs. However, the positive peaks do not have a general damping effect, most likely because of the presence of more intense peaks than in ECD.

4 Conclusion

The present contribution sketches the general philosophy and latest developments of a comprehensive research project aimed to develop a general, robust and user friendly multi-frequency spectrometer allowing *vis-à-vis* comparison between experimental and computed spectra, together with unraveling of the experimental outcome in terms of stereo-electronic, environmental, and dynamical effects. After recalling the basic aspects of our approach to vibrational (IR and VCD) spectra, we have discussed in more detail have discussed in particular integrated time dependent and time independent routes to the evaluation of vibronic effects in circular dichroism and circularly polarized luminescence spectra taking into the proper account Franck-Condon, Herzberg-Teller, Duschinsky, anharmonic, and environmental effects. As a first test case, IR and VCD anharmonic spectra of (1S,4S)-bicyclo[2,2,2]octan-2,5-dione have been computed to show that reliable results can be obtained at this level for the vibrational characteristics of ground electronic states. Next, ECD and CPL spectra of (2R,3R)–dimethyloxirane and (1R)-camphorquinone have been analyzed to point out the role of different effects, and the performance of several approximate models leading to at least semi-quantitative agreement with experiment. Of course a larger panel of cases is needed to reach general conclusions and further developments are necessary to improve the reliability of the underlying electronic computations or to treat large amplitude motions in an effective way. However, in our opinion, this and related studies show that the route is being effectively paved toward accurate yet feasible integrated experimental and theoretical studies of large systems of current technological and/or biological interest in their natural environment.

Acknowledgements

The research leading to these results has received funding from the European Union's Seventh Framework Programme (FP7/2007-2013) under grant agreement No ERC-2012-AdG-320951-DREAMS. The high performance computer facilities of the DREAMS center (http://dreamshpc.sns.it) are acknowledged for providing computer resources. The support of COST-CMTS Action CM1002 ``COnvergent Distributed Environment for Computational Spectroscopy (CODECS)'' and Gaussian, Inc. is also acknowledged.

Bibliography

[1] Circular Dichroism: Principles and Applications. Berova N, Nakanishi K, Woody RW, editors. John Wiley & Sons, Inc., 2nd ed. edition, May 2000.

[2] Crawford T. Ab initio calculation of molecular chiroptical properties. Theoretical Chemistry Accounts 2006;115:227–245.

[3] Polavarapu PL. Renaissance in chiroptical spectroscopic methods for molecular structure determination. The Chemical Record 2007;7:125–136.

[4] Autschbach J. Computing chiroptical properties with first-principles theoretical methods: Background and illustrative examples. Chirality 2009;21:E116–E152.

[5] Barone V, Improta R, Rega N. Quantum Mechanical Computations and Spectroscopy: From Small Rigid Molecules in the Gas Phase to Large Flexible Molecules in Solution. Accounts of Chemical Research 2008;41:605–616.

[6] Hujo W, Grimme S. Performance of Non-Local and Atom-Pairwise Dispersion Corrections to DFT for Structural Parameters of Molecules with Noncovalent Interactions. Journal of Chemical Theory and Computation 2013;9:308-315.

[7] Peverati R, Truhlar DG. Screened-exchange density functionals with broad accuracy for chemistry and solid-state physics. Physical Chemistry Chemical Physics 2012;14:16187–16191.

[8] Di Meo F, Trouillas P, Adamo C, Sancho-García JC. Application of recent double-hybrid density functionals to low-lying singlet-singlet excitation energies of large organic compounds. The Journal of Chemical Physics 2013;139:164104.

[9] Computational Strategies for Spectroscopy: from Small Molecules to Nano Systems. Barone V, editor. John Wiley & Sons, Inc., 2011.

[10] Tomasi J, Mennucci B, Cammi R. Quantum Mechanical Continuum Solvation Models. Chemical Reviews 2005;105:2999–3094.

[11] Rega N, Cossi M, Barone V. Structure and Magnetic Properties of Glycine Radical in Aqueous Solution at Different pH Values. Journal of the American Chemical Society 1998;120:5723–5732.

[12] Benzi C, Improta R, Scalmani G, Barone V. Quantum mechanical study of the conformational behavior of proline and 4R-hydroxyproline dipeptide analogues in vacuum and in aqueous solution. Journal of Computational Chemistry 2002;23:341–350.

[13] Egidi F, Bloino J, Cappelli C, Barone V. Development of a Virtual Spectrometer for Chiroptical Spectroscopies: The Case of Nicotine. Chirality 2013;25:701–708.

[14] Bloino J, Barone V. A second-order perturbation theory route to vibrational averages and transition properties of molecules: General formulation and application to infrared and vibrational circular dichroism spectroscopies. Journal of Chemical Physics 2012;136:124108.

[15] Barone V, Biczysko M, Bloino J. Fully anharmonic IR and Raman spectra of medium-size molecular systems: accuracy and interpretation. Physical Chemistry Chemical Physics 2014;16:1759–1787.

[16] Barone V, Baiardi A, Biczysko M, Bloino J, Cappelli C, Lipparini F. Implementation and validation of a multi-purpose virtual spectrometer for large systems in complex environments. Physical Chemistry Chemical Physics 2012;14:12404–12422.

[17] Barone V, Bloino J, Biczysko M, Santoro F. Fully Integrated Approach to Compute Vibrationally Resolved Optical Spectra: From Small Molecules to Macrosystems. Journal of Chemical Theory and Computation 2009;5:540–554.

[18] Baiardi A, Bloino J, Barone V. General Time Dependent Approach to Vibronic Spectroscopy Including Franck–Condon, Herzberg–Teller, and Duschinsky Effects. Journal of Chemical Theory and Computation 2013;9:4097–4115.

[19] Bloino J, Biczysko M, Santoro F, Barone V. General Approach to Compute Vibrationally Resolved One-Photon Electronic Spectra. Journal of Chemical Theory and Computation 2010;6:1256–1274.

[20] Cossi M, Barone V. Solvent effect on vertical electronic transitions by the polarizable continuum model. The Journal of Chemical Physics 2000;112:2427–2435.

[21] Pritchard B, Autschbach J. Calculation of the Vibrationally Resolved, Circularly Polarized Luminescence of d-Camphorquinone and (S,S)-trans-β-Hydrindanone. ChemPhysChem 2010;11:2409–2415.

[22] Pecul M, Ruud K. The optical activity of β,γ-enones in ground and excited states using circular dichroism and circularly polarized luminescence. Physical Chemistry Chemical Physics 2011;13:643–650.

[23] Emeis CA, Oosterhoff LJ. The n-π^* Absorption and Emission of Optically Active trans-β-Hydrindanone and trans-β-Thiohydrindanone. The Journal of Chemical Physics 1971;54:4809–4819.

[24] Riehl JP, Richardson FS. Circularly polarized luminescence spectroscopy. Chemical Reviews 1986;86:1–16.

[25] Emeis C, Oosterhoff L. Emission of circularly-polarised radiation by optically-active compounds. Chemical Physics Letters 1967;1:129–132.

[26] Richardson FS, Riehl JP. Circularly polarized luminescence spectroscopy. Chemical Reviews 1977;77:773–792.

[27] Luk CK, Richardson FS. Circularly polarized luminescence spectrum of camphorquinone. Journal of the American Chemical Society 1974;96:2006–2009.

[28] Condon EU. Nuclear Motions Associated with Electron Transitions in Diatomic Molecules. Physical Review 1928;32:858–872.

[29] Franck J, Dymond EG. Elementary processes of photochemical reactions. Transactions of the Faraday Society 1926;21:536–542.

[30] Condon EU. A Theory of Intensity Distribution in Band Systems. Physical Review 1926;28:1182–1201.

[31] Franck J, Weigert F, Halban Hv, Bodenstein M, Baly ECC, Lewis B, Chapman DL, Taylor HS, Allmand AJ, Christiansen JA, Bowen EJ, Noyes WA, Stern O, Norrish RGW, Flurscheim B, Marshall AL. Part II.: The mechanism of photochemical reactions. General discussion. Transactions of the Faraday Society 1926;21:581-590.

[32] Herzberg G, Teller E. Schwingungsstruktur der Elektronenübergänge bei mehratomigen Molekülen. Zeitschrift für Physikalische Chemie - Abteilung B 1933;21:410–446.

[33] Lin N, Luo Y, Santoro F, Zhao X, Rizzo A. Vibronically-induced change in the chiral response of molecules revealed by electronic circular dichroism. Chemical Physics Letters 2008;464:144–149.

[34] Duschinsky F. Acta Physicochimica URSS 1937;7:551.

[35] Ruhoff PT. Recursion relations for multi-dimensional Franck-condon overlap integrals. Chemical Physics 1994;186:355–374.

[36] Ruhoff PT, Ratner MA. Algorithms for Computing Franck-Condon Overlap Integrals. International Journal of Quantum Chemistry 2000;77:383–392.

[37] Santoro F, Improta R, Lami A, Bloino J, Barone V. Effective method to compute Franck-Condon integrals for optical spectra of large molecules in solution. Journal of Chemical Physics 2007;126:084509.

[38] Santoro F, Lami A, Improta R, Barone V. Effective method to compute vibrationally resolved optical spectra of large molecules at finite temperature in gas phase and in solution. Journal of Chemical Physics 2007;126:184102.

[39] Biczysko M, Bloino J, Santoro F, Barone V. *Computational Strategies for Spectroscopy, from Small Molecules to Nano Systems.*, John Wiley and Sons Ltd, Chichester, UK, 2011.

[40] Santoro F, Lami A, Improta R, Bloino J, Barone V. Effective method for the computation of optical spectra of large molecules at finite temperature including the Duschinsky and Herzberg-Teller effect: The Q_X band of porphyrin as a case study. Journal of Chemical Physics 2008;128:224311.

[41] Luis JM, Bishop DM, Kirtman B. A different approach for calculating Franck-Condon factors including anharmonicity. Journal of Chemical Physics 2004;120:813–822.

[42] Luis JM, Torrent-Sucarrat M, Solà M, Bishop DM, Kirtman B. Calculation of Franck-Condon factors including anharmonicity: Simulation of the $C_2H_4^+ {}^2B_{3u}$ C_2H_4 $X\,{}^1A_g$ band in the photoelectron spectrum of ethylene. Journal of Chemical Physics 2005;122:184104.

[43] Bonness S, Kirtman B, Huix M, Sanchez AJ, Luis JM. Simulation of photoelectron spectra with anharmonicity fully included: Application to the $X\,{}^2A_2$ $X\,{}^1A_1$ band of furan. Journal of Chemical Physics 2006;125:014311.

[44] Lee EPF, Mok DKW, Dyke JM, Chau FT. Ab Initio Calculations on PO_2 and Anharmonic Franckâˆ'Condon Simulations of Its Single-Vibrational-Level Emission Spectra. The Journal of Physical Chemistry A 2002;106:10130–10138.

[45] Yang L, Zhu C, Yu J, Lin SH. Anharmonic Franck–Condon simulation of the absorption and fluorescence spectra for the low-lying S_1 and S_2 excited states of pyrimidine. Chemical Physics 2012;400:126–136.

[46] Carter S, Culik SJ, Bowman JM. Vibrational self-consistent field method for many-mode systems: A new approach and application to the vibrations of CO adsorbed on Cu(100). Journal of Chemical Physics 1997;107:10548–10469.

[47] Carter S, Sharma AR, Bowman JM, Rosmus P, Tarroni R. Calculations of rovibrational energies and dipole transition intensities for polyatomic molecules using MULTIMODE. Journal of Chemical Physics 2009;131:224106.

[48] Cassam-Chena P, Liévin J. Alternative perturbation method for the molecular vibration-rotation problem. International Journal of Quantum Chemistry 2003;93:245–264.

[49] Császár AG, Fábri C, Szidarovszky T, Mátyus E, Furtenbacher T, Czakó G. The fourth age of quantum chemistry: molecules in motion. Physical Chemistry Chemical Physics 2012;14:1085–1106.

[50] Koput J, Carter S, Handy NC. Ab initio prediction of the vibrational-rotational energy levels of hydrogen peroxide and its isotopomers. Journal of Chemical Physics 2001;115:8345–8350.

[51] Carrington T, Wang XG. Computing ro-vibrational spectra of van der Waals molecules. Wiley Interdisciplinary Reviews: Computational Molecular Science 2011;1:952–963.

[52] Tennyson J. Accurate variational calculations for line lists to model the vibration–rotation spectra of hot astrophysical atmospheres.

[53] Chaban GM, Jung JO, Gerber RB. Ab initio calculation of anharmonic vibrational states of polyatomic systems: Electronic structure combined with vibrational self-consistent field. Journal of Chemical Physics 1999;111:1823–1829.

[54] Christiansen O. Vibrational structure theory: new vibrational wave function methods for calculation of anharmonic vibrational energies and vibrational contributions to molecular properties. Physical Chemistry Chemical Physics 2007;9:2942–2953.

[55] Gerber RB, Ratner MA. *Self-Consistent-Field Methods for Vibrational Excitations in Polyatomic Systems*, volume 70, John Wiley & Sons, Inc., 1988.

[56] Gregurick SK, Chaban GM, Gerber RB. Ab Initio and Improved Empirical Potentials for the Calculation of the Anharmonic Vibrational States and Intramolecular Mode Coupling of N-Methylacetamide. The Journal of Physical Chemistry A 2002;106:8696–8707.

[57] Rauhut G, Hrenar T. A combined variational and perturbational study on the vibrational spectrum of P_2F_4. Chemical Physics 2008;346:160–166.

[58] Wright NJ, Gerber RB. Direct calculation of anharmonic vibrational states of polyatomic molecules using potential energy surfaces calculated from density functional theory. Journal of Chemical Physics 2000;112:2598–2604.

[59] Wright NJ, Gerber RB, Tozer DJ. Direct calculation of anharmonic vibrational states of polyatomic molecules using density functional theory: spectroscopic tests of recently developed functionals. Chemical Physics Letters 2000;324:206–212.

[60] Bowman JM. The self-consistent-field approach to polyatomic vibrations. Accounts of Chemical Research 1986;19:202–208.

[61] Yagi K, Hirao K, Taketsugu T, Schmidt MW, Gordon MS. Ab initio vibrational state calculations with a quartic force field: Applications to H_2CO, C_2H_4, CH_3OH, CH_3CCH, and C_6H_6. Journal of Chemical Physics 2004;121:1383–1389.

[62] Clabo Jr. DA, Allen WD, Remington RB, Yamaguchi Y, Schaefer III HF. A systematic study of molecular vibrational anharmonicity and vibration-rotation interaction by self-consistent-fied higher-derivative methods. Asymmetric top molecules. Chemical Physics 1988;123:187–239.

[63] Dressler S, Thiel W. Anharmonic force fields from density functional theory. Chemical Physics Letters 1997;273:71–78.

[64] Hoy A, Mills I, Strey G. Anharmonic force constant calculations. Molecular Physics 1972;24:1265–1290.

[65] Mills IM. *Molecular Spectroscopy: Modern Research*, Academic Press, New York, 1972.

[66] Nielsen HH. The Vibration-Rotation Energies of Molecules. Reviews of Modern Physics 1951;23:90–136.

[67] Schneider W, Thiel W. Anharmonic force fields from analytic second derivatives: Method and application to methyl bromide. Chemical Physics Letters 1989;157:367–373.

[68] Willets A, Handy NC, Green Jr. WH, Jayatilaka D. Anharmonic Corrections to Vibrational Transition Intensities. Journal of Physical Chemistry 1990;94:5608–5616.

[69] Allen WD, Yamaguchi Y, Császár AG, Clabo Jr. DA, Remington RB, Schaefer III HF. A systematic study of molecular vibrational anharmonicity and vibration-rotation interaction by self-consistent-fied higher-derivative methods. Linear polyatomic molecules. Chemical Physics 1990;145:427–466.

[70] Barone V. Characterization of the potential energy surface of the HO_2 molecular system by a density functional approach. The Journal of Chemical Physics 1994;101:10666–10676.

[71] Christiansen O. Møller-Plesset perturbation theory for vibrational wave functions. Journal of Chemical Physics 2003;119:5773–5781.

[72] Neugebauer J, Hess BA. Fundamental vibrational frequencies of small polyatomic molecules from density-functional calculations and vibrational perturbation theory. Journal of Chemical Physics 2003;118:7215–7225.

[73] Ruden TA, Taylor PR, Helgaker T. Automated calculation of fundamental frequencies: Application to AlH_3 using the coupled-cluster singles-and-doubles with perturbative triples method. Journal of Chemical Physics 2003;119:1951–1960.

[74] Yagi K, Taketsugu T, Hirao K, Gordon MS. Direct vibrational self-consistent field method: Applications to H_2O and H_2CO. Journal of Chemical Physics 2000;113:1005–1017.

[75] Hermes MR, Hirata S. Second-order many-body perturbation expansions of vibrational Dyson self-energies. The Journal of Chemical Physics 2013;139:034111.

[76] Barone V. Anharmonic vibrational properties by a fully automated second-order perturbative approach. Journal of Chemical Physics 2005;122:014108.

[77] Bloino J, Biczysko M, Barone V. General Perturbative Approach for Spectroscopy, Thermodynamics, and Kinetics: Methodological Background and Benchmark Studies. Journal of Chemical Theory and Computation 2012;8:1015–1036.

[78] Bloino J, Biczysko M, Crescenzi O, Barone V. Integrated computational approach to vibrationally resolved electronic spectra: Anisole as a test case. Journal of Chemical Physics 2008;128:244105.

[79] Frisch MJ, Trucks GW, Schlegel HB, Scuseria GE, Robb MA, Cheeseman JR, Scalmani G, Barone V, Mennucci B, Petersson GA, Nakatsuji H, Caricato M, Li X, Hratchian HR, Izmaylov AF, Bloino J, Zheng G, Sonnenberg JL, Hada M, Ehara M, Toyota K, Fukuda R, Hasegawa J, Ishida M, Nakajima T, Honda Y, Kitao O, Nakai H, Vreven T, Montgomery Jr. J. A. Peralta JR, Ogliaro F, Bearpark M, Heyd JJ, Brothers E, Kudin KN, Staroverov VN, Kobayashi R, Normand J, Raghavachari K, Rendell A, Burant JC, Iyengar SS, Tomasi J, Cossi M, Rega N, Millam JM, Klene M, Knox JE, Cross JB, Bakken V, Adamo C, Jaramillo J, Gomperts R, Stratmann RE, Yazyev O, Austin AJ, Cammi R, Pomelli C, Ochterski JW, Martin RL, Morokuma K, Zakrzewski VG, Voth GA, Salvador P, Dannenberg JJ, Dapprich S, Daniels AD, Farkas O, Foresman JB, Ortiz JV, Cioslowski J, Fox DJ. Gaussian 09 Revision D.01. Gaussian Inc. Wallingford CT 2009.

[80] Becke AD. Density-functional thermochemistry. III. The role of exact exchange. Journal of Chemical Physics 1993;98:5648–5652.

[81] Double and triple-ζ basis sets of sns family, are available for download. |http://dreamslab.sns.it/downloads|.

[82] Barone V, Cimino P. Accurate and feasible computations of structural and magnetic properties of large free radicals: The PBE0/N07D model. Chemical Physics Letters 2008;454:139–143.

[83] Barone V, Cimino P. Validation of the B3LYP/N07D and PBE0/N07D Computational Models for the Calculation of Electronic g-Tensors. Journal of Chemical Theory and Computation 2009;5:192-199.

[84] Barone V, Cimino P, Stendardo E. Development and Validation of the B3LYP/N07D Computational Model for Structural Parameter and Magnetic Tensors of Large Free Radicals. Journal of Chemical Theory and Computation 2008;4:751–764.

[85] Double and triple-ζ basis sets of n07 family, are available for download. |http://idea.sns.it/downloads|.

[86] Cancès E, Mennucci B, Tomasi J. A new integral equation formalism for the polarizable continuum model: Theoretical background and applications to isotropic and anisotropic dielectrics. The Journal of Chemical Physics 1997;107:3032–3041.

[87] Kneller G. Superposition of Molecular Structures using Quaternions. Molecular Simulation 1991;7:113–119.

[88] Kneller G. Quaternions as a tool for the analysis of molecular systems. Journal de Chimie Physique 1991;88:2709–2715.

[89] Macak P, Luo Y, Ågren H. Simulations of vibronic profiles in two-photon absorption. Chemical Physics Letters 2000;330:447–457.

[90] Yanai T, Tew DP, Handy NC. A new hybrid exchange–correlation functional using the Coulomb-attenuating method (CAM-B3LYP). Chemical Physics Letters 2004;393:51–57.

[91] Zhao Y, Truhlar D. The M06 suite of density functionals for main group thermochemistry, thermochemical kinetics, noncovalent interactions, excited states, and transition elements: two new functionals and systematic testing of four M06-class functionals and 12 other functionals. Theoretical Chemistry Accounts 2008;120:215–241.

[92] Grimme S, Antony J, Ehrlich S, Krieg H. A consistent and accurate ab initio parametrization of density functional dispersion correction (DFT-D) for the 94 elements H-Pu. The Journal of Chemical Physics 2010;132:154104.

[93] Grimme S, Ehrlich S, Goerigk L. Effect of the damping function in dispersion corrected density functional theory. Journal of Computational Chemistry 2011;32:1456–1465.

[94] Longhi G, Castiglioni E, Abbate S, Lebon F, Lightner DA. Experimental and Calculated CPL Spectra and Related Spectroscopic Data of Camphor and Other Simple Chiral Bicyclic Ketones. Chirality 2013;25:589–599.

[95] Biczysko M, Panek P, Scalmani G, Bloino J, Barone V. Harmonic and Anharmonic Vibrational Frequency Calculations with the Double-Hybrid B2PLYP Method: Analytic Second Derivatives and Benchmark Studies. Journal of Chemical Theory and Computation 2010;6:2115–2125.

[96] Carbonniere P, Lucca T, Pouchan C, Rega N, Barone V. Vibrational computations beyond the harmonic approximation: Performances of the B3LYP density functional for semirigid molecules. Journal of Computational Chemistry 2005;26:384–388.

[97] Begue D, Benidar A, Pouchan C. The vibrational spectra of vinylphosphine revisited: Infrared and theoretical studies from CCSD(T) and DFT anharmonic potential. Chemical Physics Letters 2006;430:215–220.

[98] Puzzarini C, Barone V. Toward spectroscopic accuracy for organic free radicals: Molecular structure, vibrational spectrum, and magnetic properties of F_2NO. Journal of Chemical Physics 2008;129:084306.

[99] Puzzarini C, Barone V. Assessment of a computational strategy approaching spectroscopic accuracy for structure, magnetic properties and vibrational frequencies of organic free radicals: the F_2CN and F_2BO case. Physical Chemistry Chemical Physics 2008;10:6991–6997.

[100] Begue D, Carbonniere P, Pouchan C. Calculations of Vibrational Energy Levels by Using a Hybrid ab Initio and DFT Quartic Force Field: Application to Acetonitrile. The Journal of Physical Chemistry A 2005;109:4611–4616.

[101] Puzzarini C, Biczysko M, Barone V. Accurate Harmonic/Anharmonic Vibrational Frequencies for Open-Shell Systems: Performances of the B3LYP/N07D Model for Semirigid Free Radicals Benchmarked by CCSD(T) Computations. Journal of Chemical Theory and Computation 2010;6:828–838.

[102] Puzzarini C, Biczysko M, Barone V. Accurate Anharmonic Vibrational Frequencies for Uracil: The Performance of Composite Schemes and Hybrid CC/DFT Model. Journal of Chemical Theory and Computation 2011;7:3702–3710.

[103] Devlin FJ, Finley JW, Stephens PJ, Frisch MJ. Ab Initio Calculation of Vibrational Absorption and Circular Dichroism Spectra Using Density Functional Force Fields: A Comparison of Local, Nonlocal, and Hybrid Density Functionals. The Journal of Physical Chemistry 1995;99:16883–16902.

[104] Carnell M, Grimme S, Peyerimhoff S. Theoretical study of the circular dichroism and VUV spectra of trans-2,3-dimethyloxirane. Chemical Physics 1994;179:385–394.

[105] Warnke I, Furche F. Circular dichroism: electronic. Wiley Interdisciplinary Reviews: Computational Molecular Science 2012;2:150–166.

[106] Diedrich C, Grimme S. Systematic Investigation of Modern Quantum Chemical Methods to Predict Electronic Circular Dichroism Spectra. The Journal of Physical Chemistry A 2003;107:2524–2539.

[107] Pecul M, Ruud K, Helgaker T. Density functional theory calculation of electronic circular dichroism using London orbitals. Chemical Physics Letters 2004;388:110–119.

[108] Neugebauer J, Baerends EJ, Nooijen M, Autschbach J. Importance of vibronic effects on the circular dichroism spectrum of dimethyloxirane. Journal of Chemical Physics 2005;122:234305.

[109] Nooijen M. Investigation of Herzberg–Teller Franck–Condon approaches and classical simulations to include effects due to vibronic coupling in circular dichroism spectra: The case of dimethyloxirane continued. International Journal of Quantum Chemistry 2006;106:2489–2510.

[110] Breest A, Ochmann P, Pulm F, Gödderz KH, Carnell M, Hormes J. Experimental circular dichroism and VUV spectra of substituted oxiranes and thiiranes. Molecular Physics 1994;82:539–551.

[111] Autschbach J, Ziegler T, van Gisbergen SJA, Baerends EJ. Chiroptical properties from time-dependent density functional theory. I. Circular dichroism spectra of organic molecules. The Journal of Chemical Physics 2002;116:6930–6940.

Figures

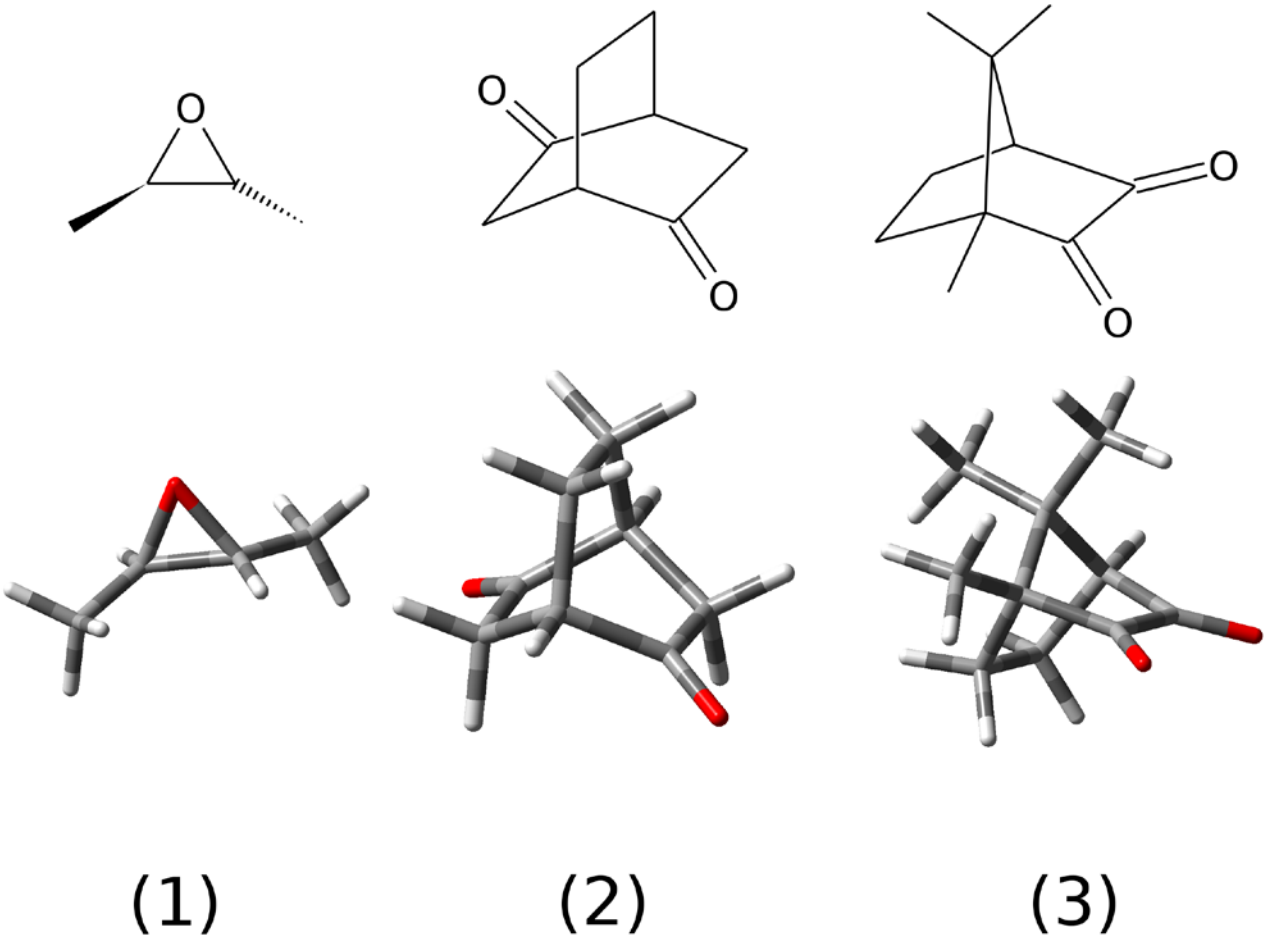

Figure 1: Skeletal formulas and 3D representation of (2R,3S)-dimethyloxirane (1); (1S,4S)-bicyclo[2,2,2]octan-2,5-dione(2); (1*R*,4*S*)-1,7,7-trimethylbicyclo[2,2,1]heptane-2,3-dione (3)

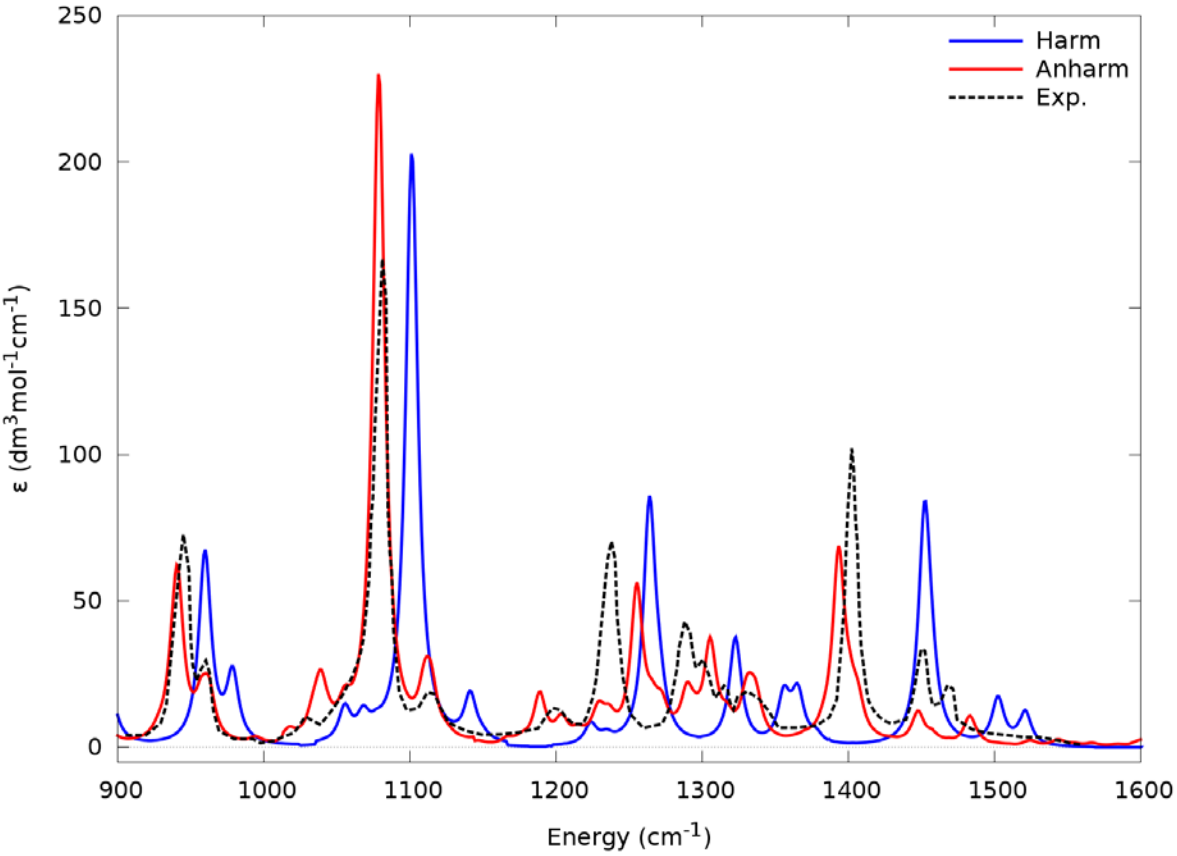

Figure 2: Simulated and experimental IR spectra of (1S,4S)-bicyclo[2.2.2]octan-2,5-dione in CCl_4. The anharmonic spectrum was calculated at the VPT2 level for both energies and intensities. Solvent effects were taken into account by using an implicit solvent model (IEF-PCM). Band broadening was simulated by applying Lorentzian functions with HWHM=5 cm^{-1}. Experimental data were taken from Ref. [94].

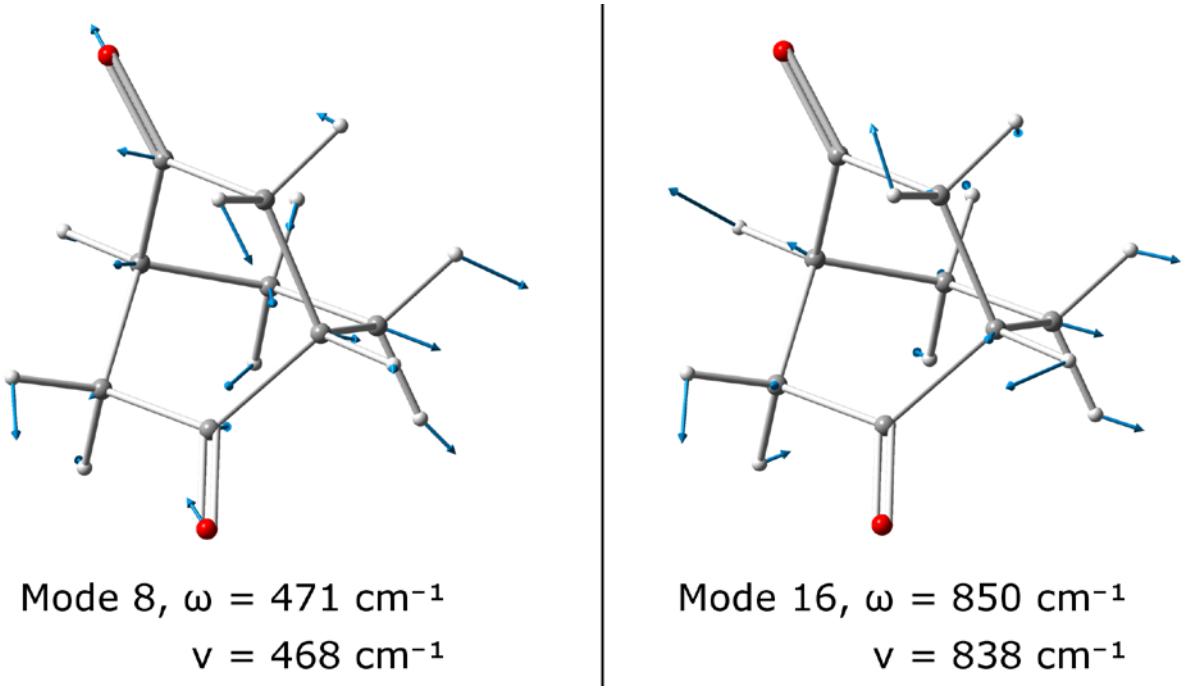

Figure 3: Graphical representation of normal modes 8 and 16 of the ground state (S_0) of (1S,4S)-bicyclo[2,2,2]octan-2,5-dione, together with their harmonic (ω) and anharmonic (ν) frequencies.

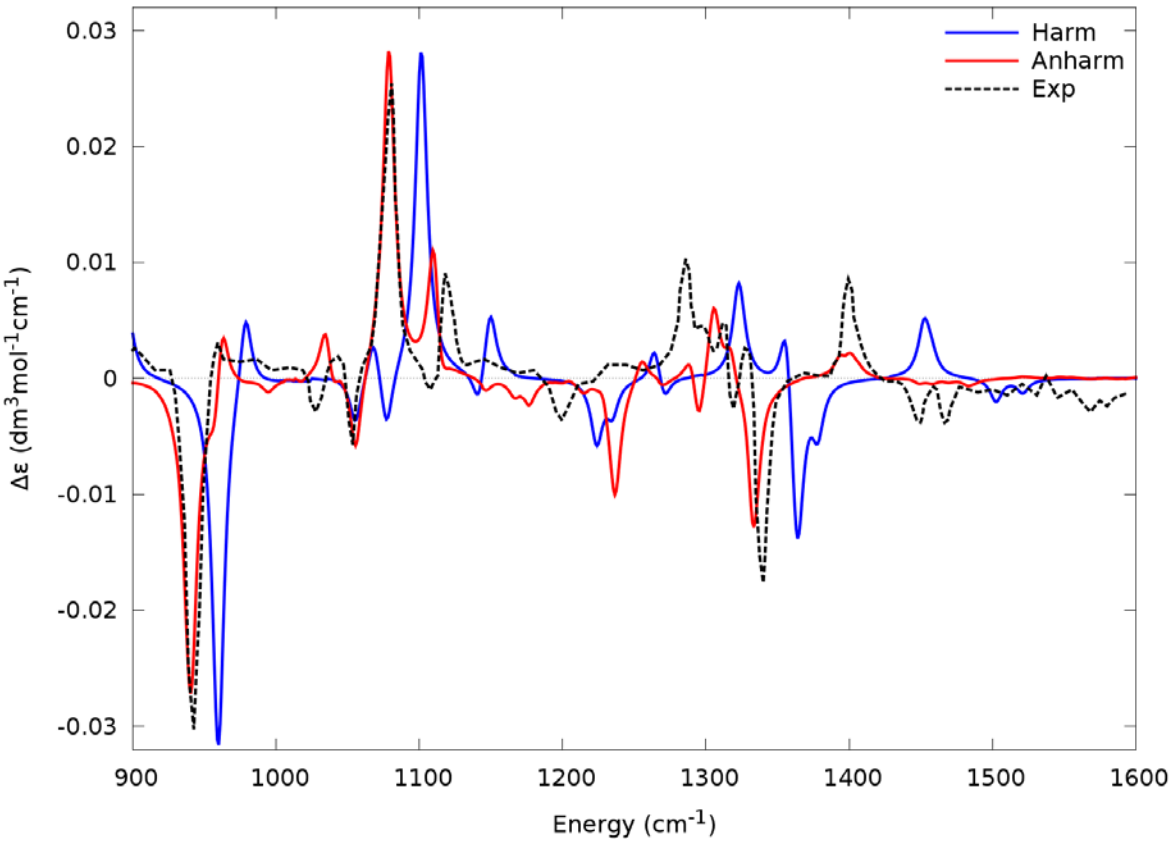

Figure 4: Simulated and experimental VCD spectra of (1S,4S)-bicyclo[2.2.2]octan-2,5-dione in CCl_4. The anharmonic spectrum was calculated at the VPT2 level for both energies and intensities. Solvent effects were taken into account by using an implicit solvent model (IEF-PCM). Band broadening was simulated by applying Lorentzian functions with HWHM=5 cm^{-1}. Experimental data were taken from Ref.[94]

[94][94]

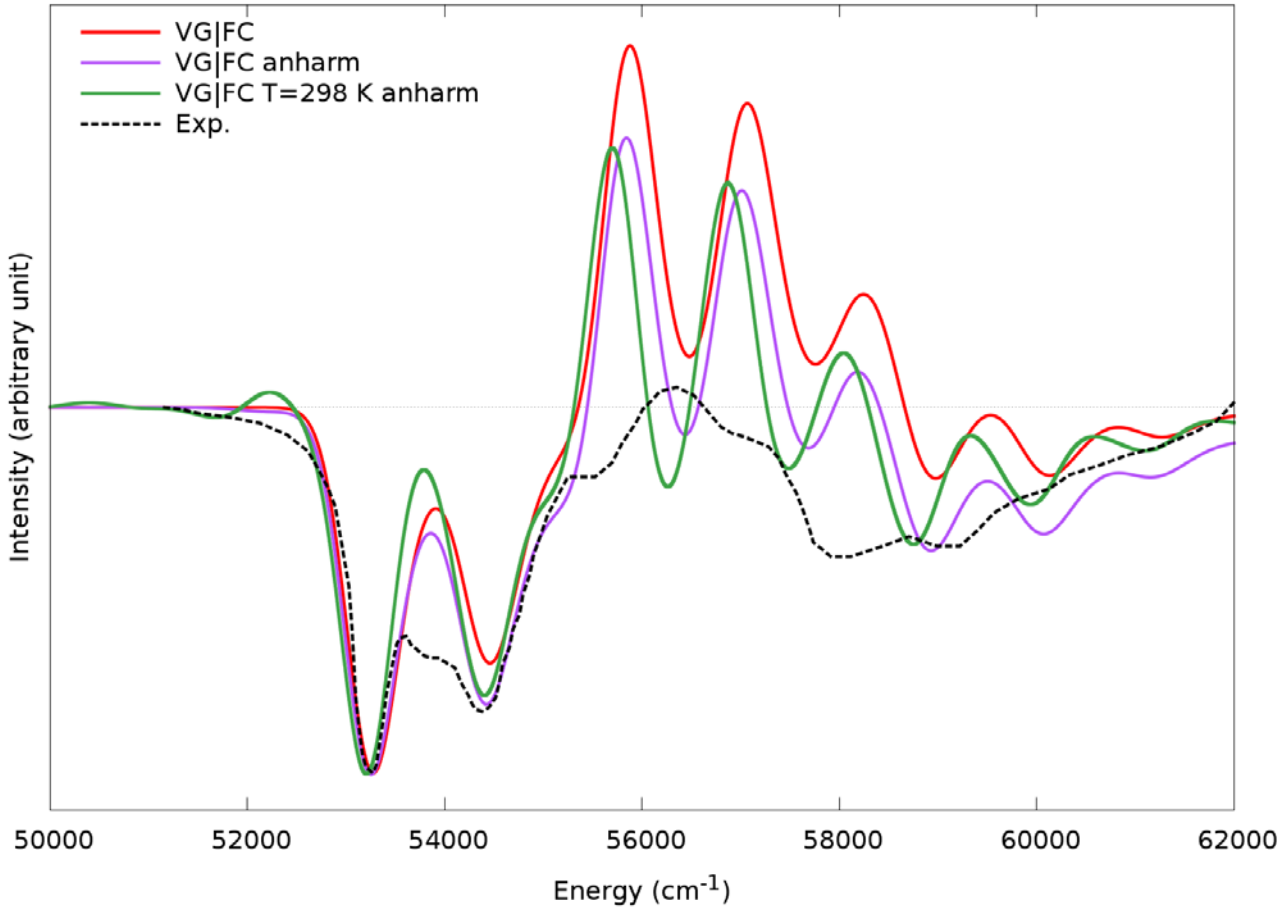

Figure 5: Simulated and experimental ECD spectrum of (2S,3S)-dimethyloxirane in vacuum. Spectra were simulated with the time-dependent approach using the vertical gradient model and the Franck-Condon approximation. Band broadening was obtained by mean of Gaussian distribution functions with half-width at half-maximum of 300 cm^{-1}. Anharmonic correction (VG|FC anharm) was included by calculating the anharmonic frequencies in the ground state and by using the mode-specific scaling scheme to extrapolate those of the excited states. Temperature effects were simulated with the time-dependent approach.

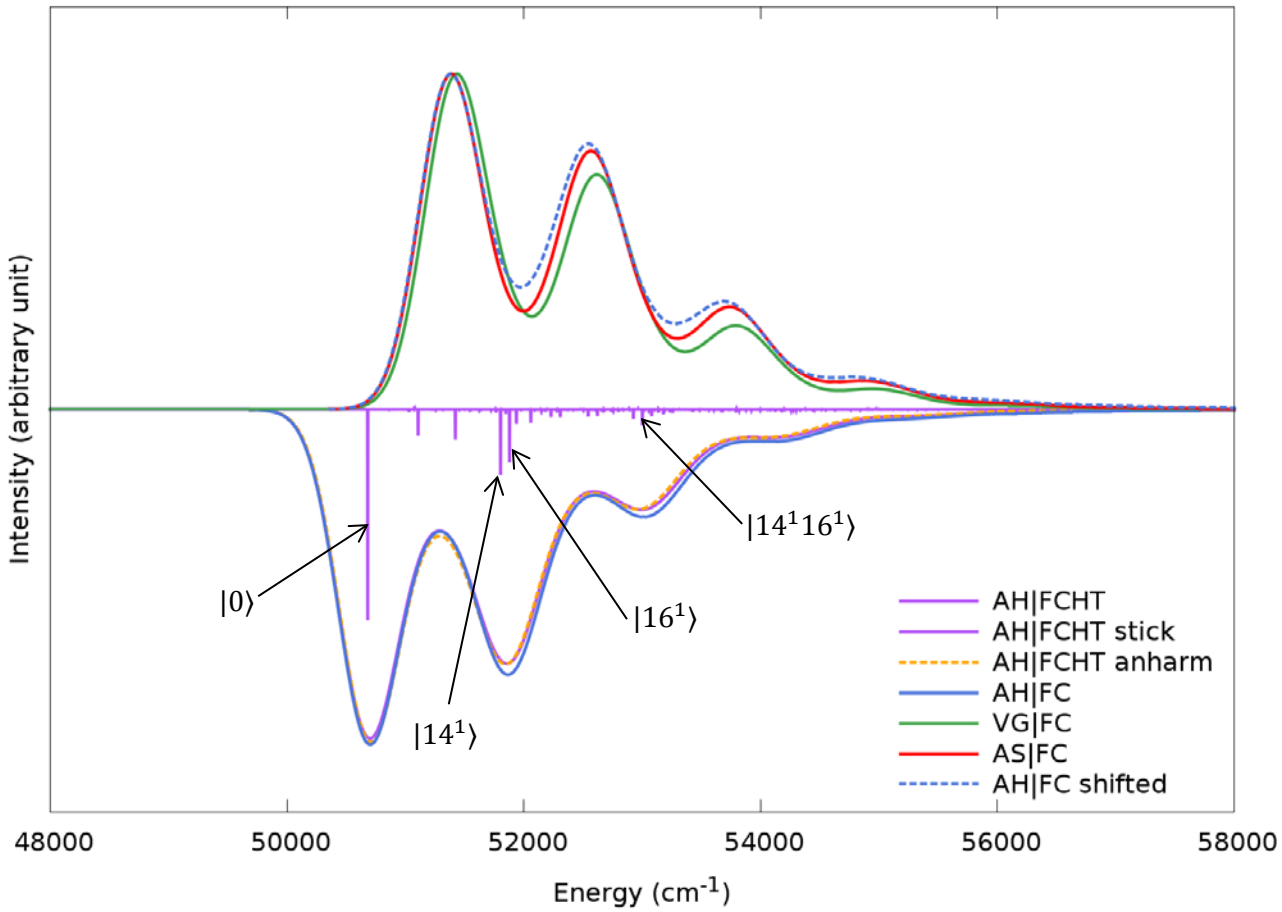

Figure 6: Simulated ECD spectra of the $S_1 \leftarrow S_0$ transition of (2R,3R)-dimethyloxirane in vacuum using the time-independent approach. Models used to generate the vibronic spectra were adiabatic hessian (AH), adiabatic shift (AS) and vertical gradient (VG), using the Franck-Condon (FC) and Herzberg-Teller (FCHT) approximation. "AH|FCHT anharm" was obtained by computing the anharmonic frequencies of the ground state and by extrapolating the excited state's ones using a mode-specific scaling scheme (see text for details). Band broadening was obtained by applying Gaussian distribution functions with HWHM=300 cm^{-1}.

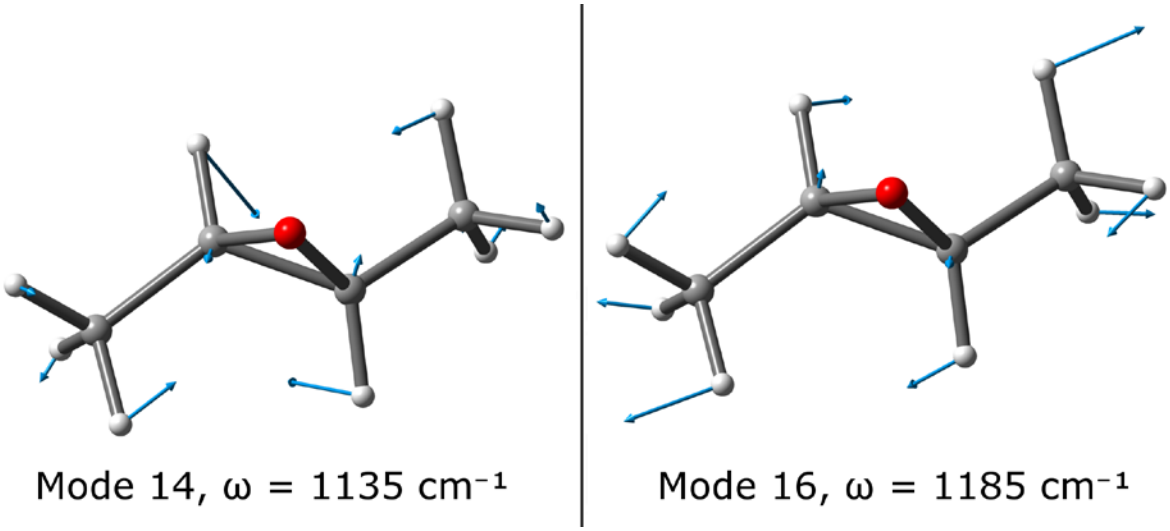

Figure 7: Graphical representation of normal modes 14 and 16 of the ground state (S_0) of (2R,3R)-dimethyloxirane and their harmonic frequencies.

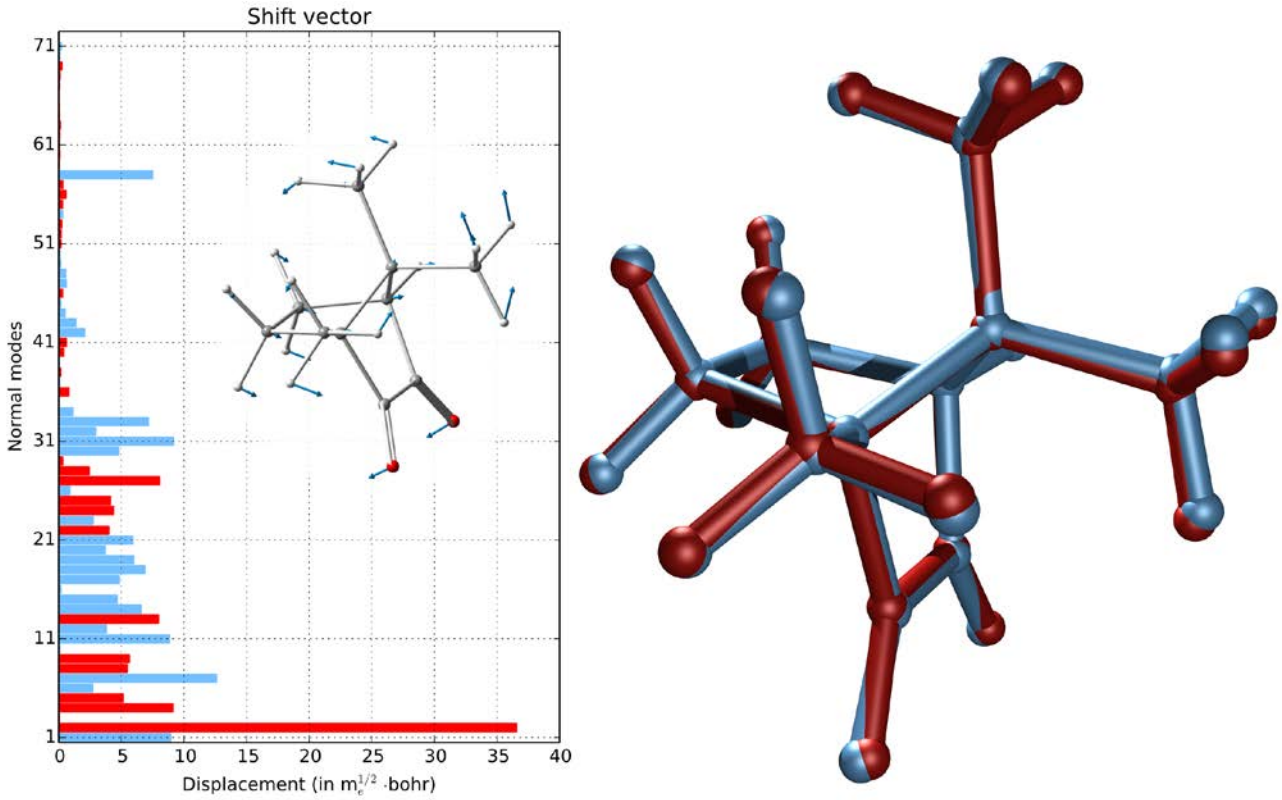

Figure 8: Shift vector (left panel) and superposed structures (right panel) associated to the $S_1 \leftarrow S_0$ transition of (1R)-camphorquinone in CCl_4.
Left panel: positive displacements are shown in clear blue and negative displacements in bright red. Mass-weighted displacements along each normal coordinate are given in atomic units (m_e represents the atomic unit of mass). Mode with the highest shift (mode 2) is represented as an inset inside the panel.
Right panel: superposed structures of the initial (clear blue) and final (dark red) electronic states. In order to highlight the atomic shifts, monochromatic representations have been chosen (see Fig. 1 for a representation of the actual atoms).

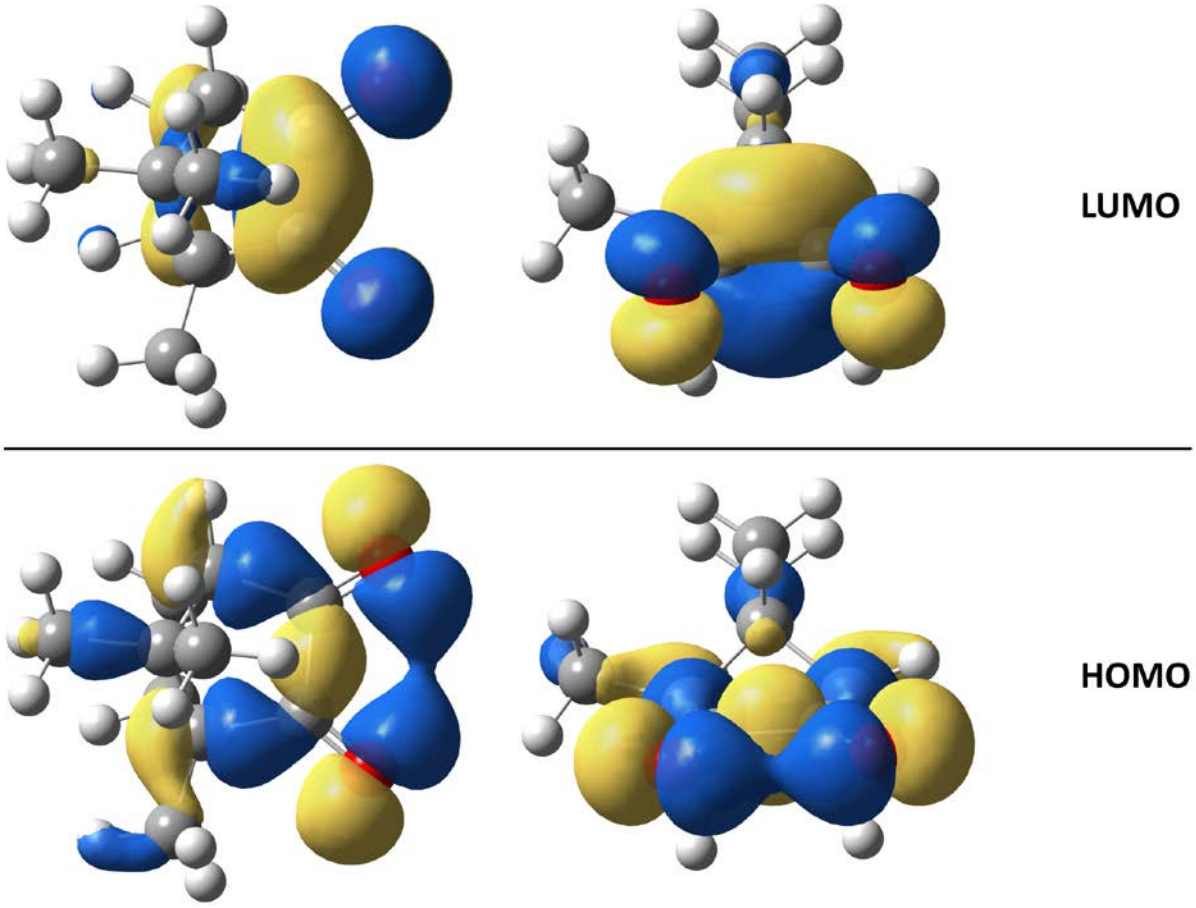

Figure 9: Frontier orbitals for the $S_1 \leftarrow S_0$ transition of (1R)-camphorquinone in CCl_4

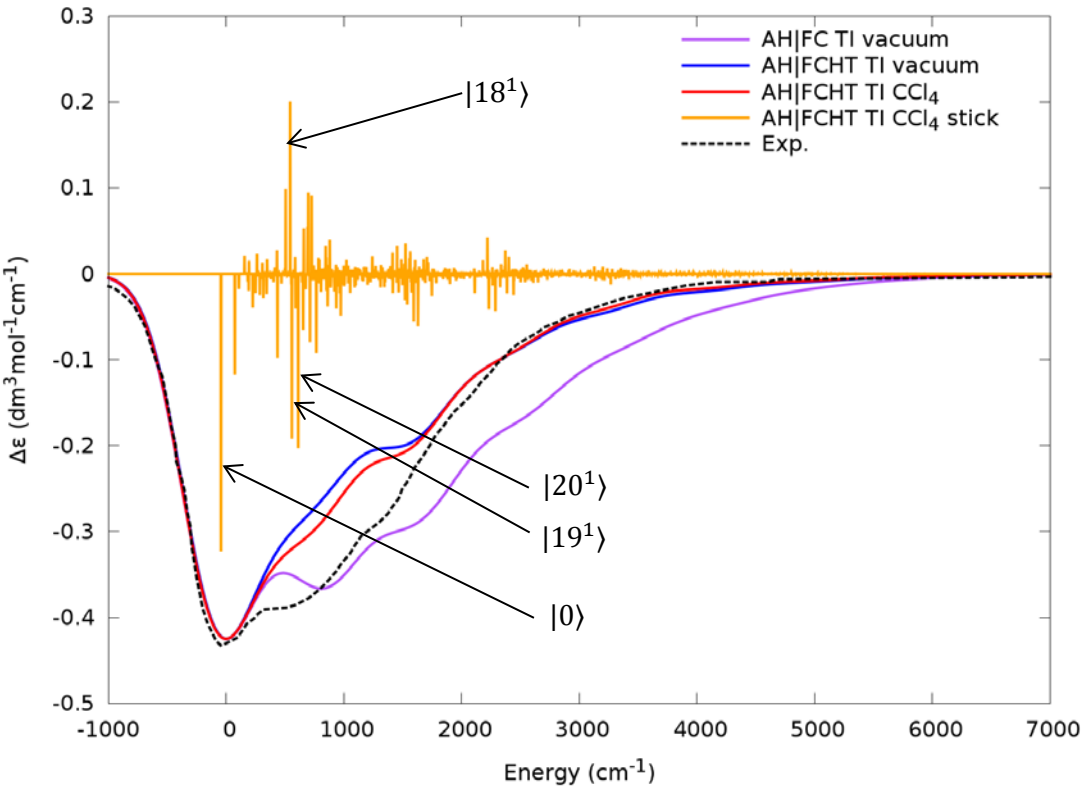

Figure 10: Simulated and experimental ECD spectra of the $S_1 \leftarrow S_0$ transition of (1R)-camphorquinone in CCl_4 and vacuum. Theoretical spectra were obtained using the time-independent (TI) approach and the adiabatic hessian (AH) model with both Franck-Condon (FC) and Herzberg-Teller (FCHT) approximations. Solvent effects were taken into account by using an implicit solvent model (IEF-PCM). Reference data were taken from Ref. [94]. Band broadening was obtained by applying Gaussian distribution functions with HWHM=350 cm^{-1}. Theoretical intensities were scaled down to fit with experimental data by dividing them with the following factors, AH|FC: 1.2, AH|FCHT (both vacuum and solvent): 1.8. For band assignment, the initial state, which is always the ground state, is omitted and only the modes with non-null quanta in the final state are indicated, with the number of quanta in superscript.

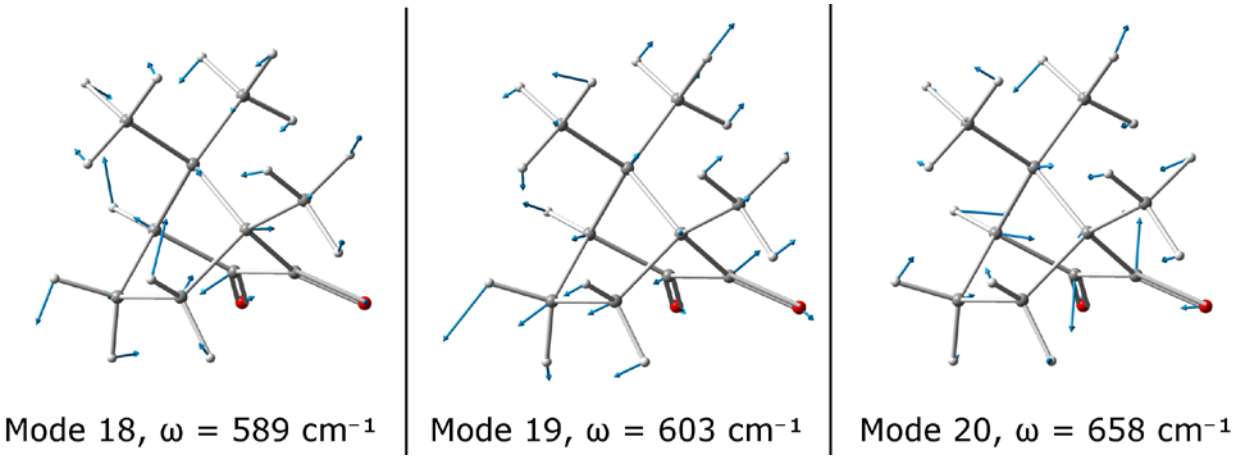

Figure 11: Graphical representation of normal modes 18, 19 and 20 of the excited state (S_1) of (1R)-camphorquinone and their harmonic frequencies.

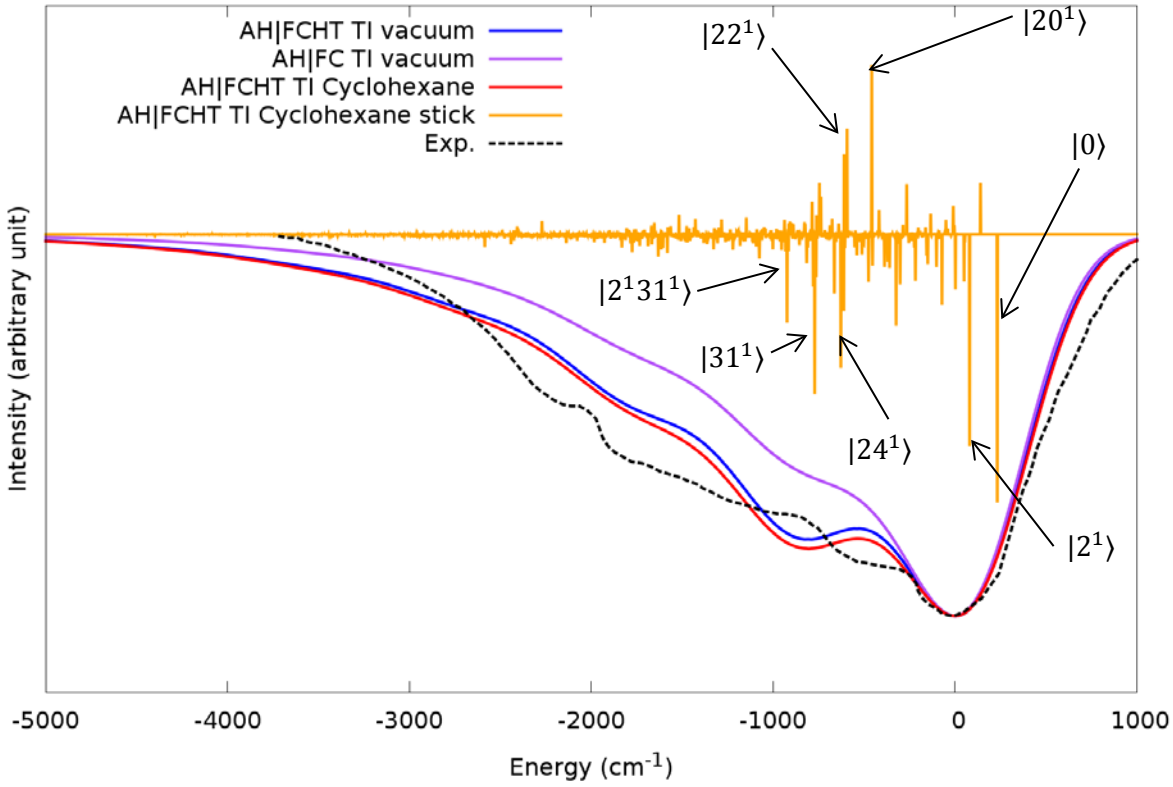

Figure 12: Simulated and experimental CPL spectra of the $S_1 \rightarrow S_0$ transition of (1R)-camphorquinone in cyclohexane and vacuum. Theoretical spectra were obtained using the time-independent (TI) approach and the adiabatic hessian (AH) model with both Franck-Condon (FC) and Herzberg-Teller (FCHT) approximations. Solvent effects were taken into account by using an implicit solvent model (IEF-PCM). Reference data were taken from Ref. [27]. Band broadening was obtained by applying Gaussian distribution functions with HWHM=350 cm^{-1}. For band assignment, the initial state, which is always the ground state, is omitted and only the modes with non-null quanta in the final state are indicated, with the number of quanta in superscript.

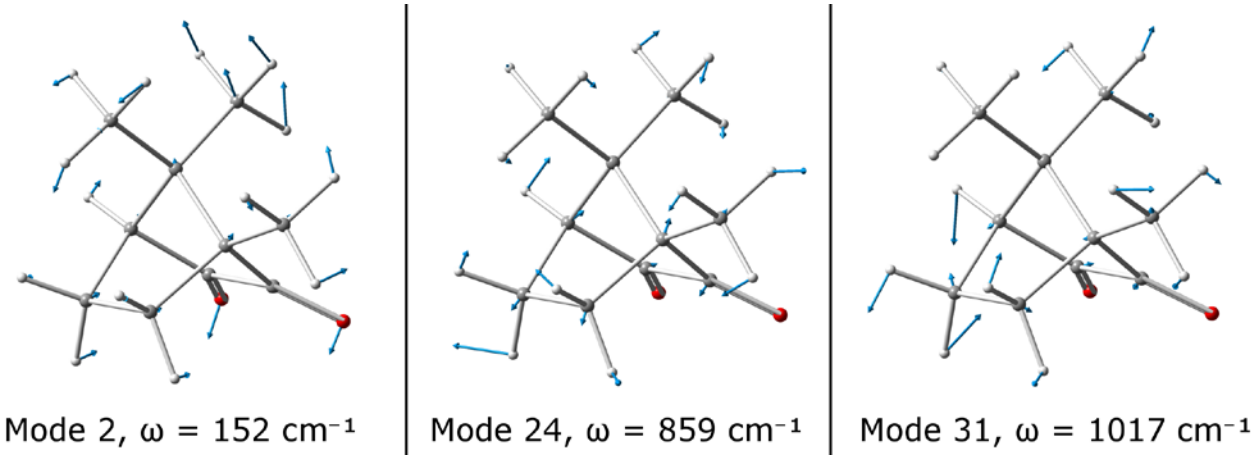

Figure 13: Graphical representation of normal modes 2, 24 and 31 of the ground state (S_0) of (1R)-camphorquinone and their harmonic frequencies.